

Supporting Information

Importance of steric bulkiness of iridium photocatalysts with PNNP tetridentate ligands for CO₂ reduction

Kenji Kamada,^a Jieun Jung,^{*a} Yohei Kametani,^b Taku Wakabayashi,^a Yoshihito Shiota,^b Kazunari Yoshizawa,^b Seong Hee Bae,^a Manami Muraki,^a Masayuki Naruto,^a Keita Sekizawa,^c Shunsuke Sato,^c Takashi Morikawa^c and Susumu Saito^{*ad}

^a Department of Chemistry, Graduate School of Science, Nagoya University, Chikusa, Nagoya 464-8602, Japan

^b Institute for Materials Chemistry and Engineering, Kyushu University, Fukuoka 819-0395, Japan.

^c Toyota Central R&D Labs., Inc., 41-1 Yokomichi, Nagakute, Aichi 480-1192, Japan

^d Integrated Research Consortium on Chemical Science (IRCCS), Nagoya University, Chikusa, Nagoya 464-8602, Japan

*To whom correspondence should be addressed.

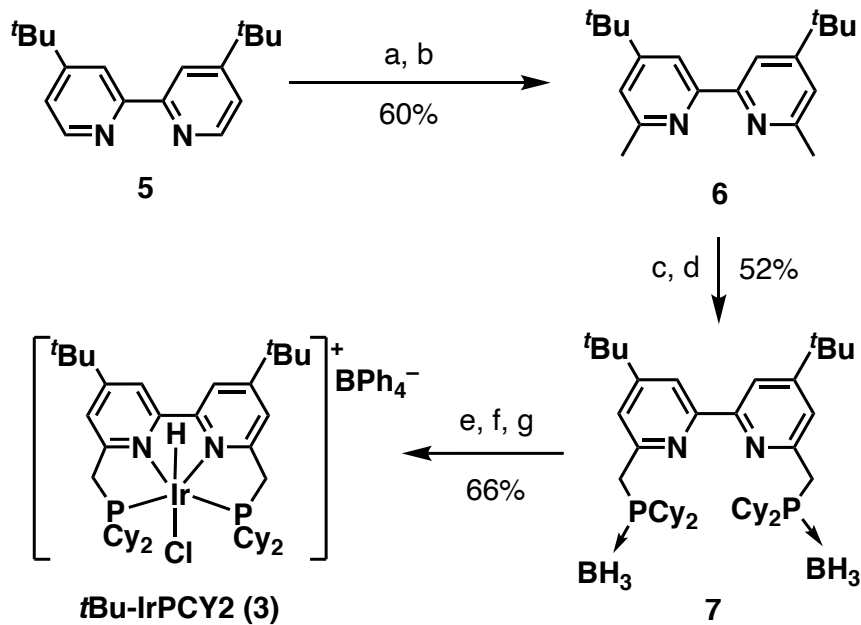
E-mail: jieun@chem.nagoya-u.ac.jp, saito.susumu@f mbox.nagoya-u.ac.jp

Experimental section

Generals. All experiments were performed under an Ar atmosphere unless otherwise noted. ¹H and ¹³C NMR spectra were recorded on a JEOL ECA-600 (600 MHz for ¹H, 151 MHz for ¹³C) at 27 °C. Chemical shifts are reported as δ in ppm and are internally referenced to tetramethylsilane (0.0 ppm for ¹H) and CDCl₃ (77.2 ppm for ¹³C). The following abbreviations are used: s = singlet, d = doublet, t = triplet, q = quartet, br = broad, dd = doublet of doublet, and m = multiplet. ³¹P NMR spectra were measured on JEOL ECA-600 (243 MHz) at ambient temperature unless otherwise noted. Chemical shifts are reported in ppm from the solvent resonance employed as the external standard (phosphoric acid (85 wt% in H₂O) at 0.0 ppm). High-resolution mass spectra (HRMS) were obtained from PE Biosystems QSTAR (ESI). For thin-layer chromatography (TLC) analysis through this work, Merck pre-coated TLC plates (silica gel 60 GF254 0.25 mm) were used. The products were purified by preparative column chromatography on silica gel 60 N (spherical, neutral) (40–100 μ m; Kanto). UV-vis spectroscopy was carried out on a Shimadzu UV-2450 spectrometer at room temperature using quartz cells (light pass length = 1.0 cm).

Materials. Commercially available chemicals were used without further purification unless otherwise indicated. Methylolithium (3 M in diethoxymethane), diisopropylamine, 1,10-phenanthroline, ammonium tetraphenylborate, and Carbon-¹³C dioxide were purchased from Aldrich Chemical Co. Morpholine, *n*-BuLi (1.6 M in hexane), *N,N*-dimethylacetamide (anhydrous), THF (anhydrous), methanol (anhydrous), diethyl ether (anhydrous), ethyl acetate, chloroform, deuterium oxide and celite were purchased from Kanto Chemicals, Ltd. Borane–tetrahydrofuran complex, triethanolamine, ethanol (anhydrous), chlorodicyclohexylphosphine, chloroform-*d*, and hexane were purchased from FUJIFILM Wako Pure Chemical Corporation. Tetraethylammonium tetrafluoroborate was purchased from Tokyo Chemical Industry CO., Ltd. Chloro(1,5-cyclooctadiene)iridium(I) dimer was purchased from FURUYA METAL CO., LTD. Manganese(IV) dioxide was purchased from Merck. Carbon dioxide gas was purchased from Alpha system Co., Ltd. *N,N*-dimethylacetamide-*d*₉ was purchased from Cambridge Isotope Laboratories. Inc. 1,3-dimethyl-2-phenyl-2,3-dihydro-1*H*-benzo[*d*]imidazole (BIH) was synthesized according to the literature.^{S1} IrPIP2 (**1**), IrPCY2 (**2**) and Mes-IrPCY2 (**4**) were synthesized according to the literatures.^{S2–S3}

Instrumentation. Products obtained in the photocatalytic reduction of CO₂ were analyzed by Micro-GC (Agilent 490) equipped with a thermal conductivity detector (column: MS5A 10-m BF column; isothermal at 80 °C; carrier gas: Ar), and Prominence Organic Acid Analysis System (SCR-102H Column; Column Temp.: 40 °C; Cell Temp.: 43 °C) or IC instrument (Dionex ICS-2000) with IonPacAS15 and Ion-PacAG15 columns. The column temperature was maintained at 308 K. A solution of 3 mM KOH was used as the first eluent up to 10 min, and then the eluent was changed gradually to 10 mM KOH over 5 min, followed by a change to 30 mM KOH solution over 5 min. Sub-nanosecond laser-induced transient absorption spectra were collected by a customized measuring system (picoTAS, Unisoku Co., Ltd.), which is based on a Randomly-Interleaved-Pulse-Train method.^{S4} The pump laser used is a passive Q-SW YAG laser (Powerchip 355 nm, TeemPhotonics), of which pulse width is 350 ps. Cyclic voltammetry (CV) and differential pulse voltammetry (DPV) measurements were carried out in DMA containing 0.10 M tetrabutylammonium tetrafluoroborate (Et₄NBF₄) as an electrolyte at 298 K under Ar with use of a glassy carbon as a working electrode (3 mm diameter), a platinum wire as a counter electrode and a Ag/AgNO₃ electrode (in CH₃CN solution containing 0.10 M tetrabutylammonium perchlorate and 0.01 M AgNO₃). The potentials were calibrated by the standard potential of ferrocene/ferrocenium (Fc/Fc⁺).



Scheme S1. The synthesis of *t*Bu-IrPCY2 (3). Reagents: a) MeLi, THF; b) MnO₂, CH₂Cl₂; c) LDA, PCy₂Cl, THF; d) BH₃–THF; e) Morpholine; f) [Ir(cod)Cl]₂, MeOH; g) NH₄BPh₄, MeOH

Synthesis of 4,4'-di-*tert*-butyl-6,6'-dimethyl-2,2'-bipyridine (6). In a 300 mL two-necked flask, 4,4'-bis(*tert*-butyl)-2,2'-bipyridine (2.6864 g, 10.0 mmol), anhydrous THF (66 mL) and magnetic stirring bar were placed under an Ar atmosphere. To the solution was added 3 M methylolithium (15 mL, 45 mmol) at -61 °C. The resulting solution was stirred at this temperature for 1 h and then warmed to 0 °C. After overnight at this temperature, the mixture was refluxed 4 h at 80 °C. Then pure water (14 mL) was added to the reaction mixture at 0 °C and organic phase was evaporated. Following extraction with CH₂Cl₂ (40 mL × 3), the organic layer was dried with Na₂SO₄ and filtered. To the filtrate was added MnO₂ (26.4324 g) at room temperature. After stirring 0.5 h, the mixture was filtered over celite and evaporated. The crude product was purified by column chromatography (SiO₂, AcOEt:hexane = 1:8) to afford target compound as white solid (1.8045 g, 60% yield). ¹H NMR (600 MHz, CDCl₃): δ 8.13 (d, 2H, *J* = 1.8 Hz, C₁₀H₄N₂), 7.14 (d, 2H, *J* = 1.8 Hz, C₁₀H₄N₂), 2.63 (s, 6H, CH₃), 1.36 (s, 18H, C(CH₃)₃). ¹³C{¹H} NMR (151 MHz, CDCl₃): δ 161.1, 157.8, 156.7, 120.2, 115.8, 35.0, 30.8, 25.0. HRMS (ESI, (M+H)⁺) Calcd for C₂₀H₂₉N₂⁺: 297.2331. Found: 297.2320.

Synthesis of 6,6'-bis((dicyclohexylphosphino)methyl)-4,4'-di-*tert*-butyl-2,2'-bipyridine–diborane complex (7). In a 300 mL two-necked flask, 4,4'-di-*tert*-butyl-6,6'-dimethyl-2,2'-bipyridine (1.4840 g, 5.0 mmol), anhydrous THF (25 mL) and magnetic stirring bar were placed under an Ar atmosphere. The flask was immersed in an ice bath and stirred at 0 °C. To the solution was added LDA (prepared by mixing diisopropylamine (4.21 mL, 30 mmol), *n*-BuLi (1.6 M in hexane, 18.8 mL), and 15 mL anhydrous THF for 10 min stirred at 0 °C). The resulting solution was stirred for 1 h at room temperature. To the solution was added chlorodicyclohexylphosphine (2.2 mL, 10 mmol) dropwise to the solution at 0 °C. After stirring for 18.5 h at room temperature, to the solution was added BH₃–THF solution (1 M in THF, 50 mL, 50 mmol). After stirring at room temperature for 23 h, the reaction mixture was quenched by 50 mL water at 0 °C, and the organic phase was evaporated. After extraction with CH₂Cl₂ (50 mL × 3), the organic layer was dried over Na₂SO₄ and filtered. The solvent was evaporated, and the residue was washed with ethyl acetate to afford the target compound as white solid (1.907 g, 52% yield). ¹H NMR (600 MHz, CDCl₃): δ 8.33 (s, 2H, C₁₀H₄N₂), 7.32 (s, 2H, C₁₀H₄N₂), 3.34 (d, 4H, *J* = 11.4 Hz, PCH₂), 1.89–1.11 (m, 62H, C(CH₃)₃, C₆H₁₁), 0.55 (br, 6H, BH₃). ¹³C{¹H} NMR (151 MHz, CDCl₃): δ 161.4, 155.7, 154.1 (d), 122.5, 116.1, 35.1, 31.8 (d), 31.0 (d), 30.7, 27.24, 27.17, 27.1, 26.8, 26.7, 26.1. ³¹P{¹H} NMR (243 MHz, CDCl₃): δ 28.5. HRMS (ESI, (M+H)⁺) Calcd for C₄₄H₇₇B₂N₂P₂⁺: 717.5748. Found: 717.5729.

Synthesis of *t*Bu-IrPCY2 (3). In a vessel equipped with a young stopcock, 6,6'-bis((dicyclohexylphosphino)methyl)-4,4'-di-*tert*-butyl-2,2'-bipyridine–diborane complex (0.1444 g, 0.20 mmol), degassed morpholine (6 mL), and magnetic stirring bar were placed under an Ar atmosphere. The mixture was stirred at 120 °C in 2 h and cooled to room temperature, before morpholine was removed *in vacuo* (ca. 0.1 mmHg, 70 °C). To the residue was added chloro(1,5-cyclooctadiene)iridium(I) dimer (0.0672 g, 0.10 mmol) and degassed methanol (7.2 mL). The resulting mixture was heated at 70 °C for 12 h, and then cooled down to room temperature. After the mixture was filtered through a pad of celite under an Ar atmosphere, ammonium tetraphenylborate (0.4770 g, 0.30 mmol) was added to the filtrate to afford yellow precipitation. The suspension was stirred for 21 h at room temperature. The precipitation was collected by filtration and washed with methanol and Et₂O. The residue was purified by recrystallization from slow diffusion of degassed MeOH into CH₂Cl₂ solution of the compound at room temperature to afford *t*Bu-IrPCY2 as a yellow crystal (0.1624 g, 66% yield). ¹H NMR (600 MHz, CDCl₃): δ 7.76 (s, 2H, C₁₀H₄N₂), 7.54 (s, 2H, C₁₀H₄N₂), 7.46 (m, 8H, B(C₆H₅)₄), 7.02 (t, 8H, *J* = 7.4 Hz, B(C₆H₅)₄), 6.87 (t, 4H, *J* = 7.4 Hz, B(C₆H₅)₄), 3.65 (dd, 2H, *J* = 17.4, 9.0 Hz, PCH₂), 3.38 (dd, 2H, *J* = 17.4, 10.2 Hz, PCH₂), 2.41 (m, 2H, C₆H₁₁), 2.19 (m, 2H, C₆H₁₁), 1.91–1.66 (br, 18H, C₆H₁₁), 1.52–0.92 (br, 40H, C₆H₁₁, C(CH₃)₃), –21.2 (t, 1H, *J* = 18.4 Hz, IrH). ¹³C{¹H} NMR (151 MHz, CDCl₃): δ 164.51 (q), 164.48, 161.2, 156.1, 136.4, 125.7 (m), 121.8, 121.3, 119.1, 39.2 (d), 36.1, 35.8 (t), 30.6, 28.8, 28.6, 28.2, 27.7, 27.2 (m), 26.5 (m), 26.2 (m), 26.1, 26.0. ³¹P{¹H} NMR (243 MHz, CDCl₃): δ 20.0. HRMS (ESI, (M–BPh₄)⁺) Calcd for C₄₄H₇₁ClIrN₂P₂⁺: 917.4410. Found *m/z* = 917.4417. Anal. Calcd. for C₆₈H₉₁B₁Cl₁Ir₁N₂P₂: C 66.03, H 7.42, N 2.26, found: C 65.87, H 7.22, N 2.56.

Kinetic measurements. The reactions were run in a 1.0 cm quartz cuvette and followed by monitoring transient absorption spectral changes (excited at 355 nm) of the reaction solutions of **1** (2.0 mM), **2** (2.0 mM) or **3** (1.5 mM) in the presence of BIH (0–4 mM) in DMA at 298 K. The same procedure was used for spectral measurements for oxidation of other substrates with an Ir complex. Second-order rate constants were determined under pseudo-first-order conditions (i.e., [substrate]/[Ir] > 10) by fitting the changes in transient absorbance for the decay of peaks due to the excited Ir complexes in the oxidation reactions of substrates (0.25–100 mM) in DMA at 298 K. Reactions of Ir complexes with substrates were monitored by the changes in the absorption bands at 480 nm for **1** and **2**, or at 500 nm for **3**.

Product analysis. Photocatalytic reactions were performed at atmospheric pressure in 8 mL test tubes containing 4 mL of a DMA/H₂O/TEOA (9:1:2, v/v/v) solution purged with CO₂ for 10 min in the presence of an Ir complex. The reaction solution of Ir complexes with BIH in 8 mL test tubes were prepared at atmospheric pressure by mixing a CO₂-saturated mixture of DMA/H₂O solution containing Ir complexes and a CO₂-saturated DMA solution containing BIH. The reaction solution of **4** with BIH in 35 mL test tubes were prepared at atmospheric pressure by mixing a CO₂-saturated DMA/H₂O solution containing **4** and a degassed DMA solution containing BIH. The resulting mixed solution of a DMA/H₂O (9:1, v/v) containing **4** and BIH were purged with CO₂ for 20 min. The stock solution of **4** was prepared under air, immediately transferred to test tubes and purged with CO₂. The solutions were irradiated in a turntable irradiation apparatus at room temperature using a Xe lamp (300 W) combined with a UV-cut filter having a cut-off wavelength of below 400 nm and a UV and IR cut filter ranging from 385 nm to 740 nm. The gaseous reaction products were analyzed using a micro-GC (Agilent 490) equipped with a thermal conductivity detector (column: MS5A 10-m BF column; isothermal at 80 °C; carrier gas: Ar), and the products in the solution were analyzed using Prominence Organic Acid Analysis System (SCR-102H Column; Column Temp.: 40 °C; Cell Temp.: 43 °C) or IC instrument (Dionex ICS-2000) with IonPacAS15 and Ion-PacAG15 columns. The column temperature was maintained at 308 K. A solution of 3.0 mM KOH was used as the first eluent up to 10 min, and then the eluent was changed gradually to 10 mM KOH over 5 min, followed by a change to 30 mM KOH solution over 5 min.

Quantum yield determination. A quantum yield (Φ) of photocatalytic reduction of CO₂ in an CO₂-saturated mixture of DMA/H₂O/TEOA (9:1:2, v/v/v; 4.0 mL) containing an Ir complex was determined under visible light irradiation of monochromatized light using a Xe lamp (300 W) on an ASAHI SPECTRA MAX-303 through a band-pass filter transmitting $\lambda = 400$ nm at 298 K. The amount of HCO₂H and CO produced during the photochemical reaction was determined under photoradiation ($\lambda = 400$ nm) with irradiation time interval of 2 h (Fig. S3). The slope of the graph in 2–10 h for HCO₂H and 4–10 h for CO is taken to determine the quantum yield. The quantum yield was determined using the following equation, $\Phi (\%) = (2 \times R/I) \times 100$, where R (mol s⁻¹) is the rate of the formation of HCO₂H and CO, and I (einstein s⁻¹) is the rate of photon flux of the incident light. The total number of incident photons was determined using a standard actinometer as follows. A test tube containing an aqueous solution (4.0 mL) of potassium ferrioxalate (K₃[Fe^{III}(C₂O₄)₃]: 6.0 mM) was irradiated using monochromatized light ($\lambda = 400$ nm) for 1, 2 and 3 min at 298 K. At the end of the irradiation, a sodium acetate buffer solution (2.0 mL) of phenanthroline was added to 1.0 mL of the actinometer solution and the solution was kept under dark for 1 h. The absorbance at 510 nm due to [Fe(phen)₃]²⁺ ($\varepsilon = 11050$ M⁻¹ cm⁻¹ at $\lambda_{\text{max}} = 510$ nm) was measured to determine the total number of incident photons using the quantum yield for the photodecomposition of ferrioxalate ($\Phi = 1.14$ at 405–407 nm)^{S5} to be 2.02×10^{-9} einstein s⁻¹ [rate of formation of [Fe(phen)₃]²⁺ after dilution = 2.12×10^{-3} (slope of a inset) / 11050 (ε) = 1.92×10^{-7} M s⁻¹ and rate of formation of [Fe(phen)₃]²⁺ before dilution = 1.92×10^{-7} M s⁻¹ × (4 × 10⁻³ L) × 3 (rate of dilution) = 2.31×10^{-9} mol s⁻¹, $I = 2.31 \times 10^{-9}/1.14 = 2.02 \times 10^{-9}$ einstein s⁻¹]. The same measurements were repeated twice more, and the average value of them is 2.00×10^{-9} einstein s⁻¹. Because the percentage of light absorption of actinometer solution is 96.8%, the total number of incident photons is 2.07×10^{-9} einstein s⁻¹ (Fig. S3b). The quantum yields of the production of HCO₂H and CO were calculated by following equation: QY (%) = $(2 \times R/I) \times 100\%$, where R is the evolution rate of HCO₂H and CO, and I is the rate of photon flux irradiated to the reaction mixture (2.07×10^{-9} einstein s⁻¹).

DFT calculation. All optimized structures were obtained using the B3LYP functional^{S6,S7} as implemented in Gaussian 16 packages.^{S8} SDD and D95** basis set^{S9,S10} were used for the Ir atom and the other atoms (H, C, N, O, P, and Cl), respectively. Using the vibrational frequency analysis, we confirmed that the obtained local minima have none imaginary frequency. To simulate UV-vis spectra, TD-DFT^{S11} calculations were performed using the ωB97XD^{S12} functional with optimized structures of the B3LYP functional.

Table S1 Photocatalytic systems for CO₂ reduction using a self-photosensitized catalyst

Catalyst	Electron donor	Irradiation, nm	Product	TON, (Time, h)	TOF, h ⁻¹	Ref.
1	20 μM	BIH	λ ≥ 400	HCO ₂ H CO	399 (48) 294 (48)	8.3 6.1
2	20 μM	BIH	λ ≥ 400	HCO ₂ H CO	543 (48) 116 (48)	11 2.4
3	20 μM	BIH	λ ≥ 400	HCO ₂ H CO	449 (48) 97 (48)	9.4 2.0
4^a	20 μM	BIH	λ ≥ 400	HCO ₂ H CO	7373 (168) 3114 (168)	44 18
	100 μM	BIH	λ ≥ 400	HCO ₂ H CO	1231 (18) 82 (18)	68 5
[Ir(tpy)(Meppy)-Cl] ⁺	0.50 mM	TEOA	410 ≤ λ ≤ 750	CO	ca.105 (4)	S13
[(Ir(tpy)(ppy)I) ₂ -(CH ₂) ₂] ²⁺	0.17 mM	TEOA	λ = 450	CO	135 (ca.8)	S14
[Ir((9-anthryl)-tpy)(ppy)Cl] ⁺	0.50 mM	TEOA	λ = 450	CO	265 (255)	S15
[Ir(tpy)(bpy)Cl] ⁺	0.50 mM	TEOA	410 ≤ λ ≤ 750	HCO ₂ H CO	20 (24) 2 (24)	0.8 0.1
Re(bpy)(CO) ₃ Cl	0.87 mM	TEOA	λ ≥ 400	CO	27 (4)	S17
Re(pyNHC-PhCF ₃)(CO) ₃ Br	0.10 mM	BIH	Solar simulator	CO	32 (4)	S18
[Re(bpy)(NS-carbene)(CO) ₂] ⁺	0.50 mM	BIH	λ ≥ 480	CO	153 (15)	S19
[Re(bpy) ₂ (CO) ₂] ⁺	1.0 mM	TEOA	λ = 405	HCO ₂ H	10 (24)	0.43
[Ru(tpy)(cpic)(MeCN)] ²⁺	20 μM	BIH	420 ≤ λ ≤ 750	CO	110 (3)	S21
[Ru(tpy)(pqn)-(MeCN)] ²⁺	40 μM	BIH TEOA	420 ≤ λ ≤ 750	CO HCO ₂ H	160 (11) 14 (4)	15 3.5
Ru(CNC)(bpy)-(MeCN)	1.0 nM	BIH	Solar simulator	CO	33000 (20)	S23
Os(dtbbpy)(CO) ₂ Cl ₂	0.50 mM	TEOA	λ ≥ 326	HCO ₂ H CO	8 (14) 47 (14)	0.6 3.4
FeTPP (CAT)	10–50 μM	TEA	λ > 280	CO	30 (10)	S25
Fe-p-TMA	2 μM	BIH	λ ≥ 420	CO	101 (102)	S26
CoTPP	10 μM	TEA	λ ≥ 320	HCO ₂ H CO	320 (190) 80 (190)	1.7 0.4

^a [BIH], 0.25 M was used.

Table S2 Calculated TD-DFT excitation energies of Ir complexes. *f* denotes the oscillator strength calculated for each transition

Complex	λ , nm	<i>f</i>	Transition
1	350	0.0254	HOMO → LUMO
2	358	0.0245	HOMO → LUMO
3	341	0.0378	HOMO → LUMO
4	344	0.0471	HOMO → LUMO

Table S3 One-electron oxidation potentials (E_{ox}) of reductants and second-order rate constants of electron transfer (k_{et}) from reductants to the excited state of an Ir complex ($\lambda_{\text{ex}} = 355$ nm) in a deaerated DMA solution at 298 K

Reductant	E_{ox} , V vs SCE ^a	Complex 1 $k_{\text{et}}, \text{M}^{-1} \text{s}^{-1}$	Complex 2 $k_{\text{et}}, \text{M}^{-1} \text{s}^{-1}$	Complex 3 $k_{\text{et}}, \text{M}^{-1} \text{s}^{-1}$	Complex 4 ^{S3} $k_{\text{et}}, \text{M}^{-1} \text{s}^{-1}$
1,4-dimethoxybenzene	1.24	9.80×10^7	5.30×10^7	2.26×10^7	2.83×10^7
1,2,3,4-tetramethoxybenzene	1.17	1.64×10^8	1.07×10^8	6.23×10^7	4.90×10^7
1,2,4-trimethoxybenzene	0.96	7.29×10^8	9.26×10^8	5.97×10^8	5.02×10^8
triphenylamine	0.83	1.11×10^9	1.20×10^9	9.64×10^8	9.32×10^8
bromoferrocene	0.54	3.06×10^9	2.95×10^9	2.36×10^9	2.33×10^9
ferrocene	0.37	3.98×10^9	3.95×10^9	3.26×10^9	3.17×10^9

^a One-electron oxidation potentials of reductants were determined by cyclic voltammetry (CV) and differential pulse voltammetry (DPV) in a DMA solution containing 0.10 M of Et₄NBF₄ at 298 K.

Table S4 Cartesian coordinates of **1**

Atom	x	y	z
Ir	-0.101633	-0.143189	-0.007613
P	2.205505	-0.554475	0.032984
Cl	-0.084054	-0.319815	-2.546288
P	-0.681917	2.125545	0.125226
N	-0.261739	-2.218793	0.026111
N	-2.166447	-0.398552	-0.087719
C	-1.531486	-2.70318	0.120975
C	-2.60166	-1.682621	0.037823
C	-1.758679	-4.076687	0.245521
H	-2.767414	-4.466126	0.330028
C	3.21198	-0.468581	1.621417
H	4.101511	-1.075385	1.404048
C	0.803847	-3.043833	-0.018003
C	-3.028812	0.621213	-0.286919
C	-0.662799	-4.946652	0.255634
H	-0.817039	-6.017748	0.358623
C	0.627623	-4.429379	0.111322
H	1.492033	-5.086659	0.083592
C	-3.96978	-1.970437	0.033399
H	-4.321967	-2.99094	0.137308
C	-2.429669	1.977972	-0.564691
H	-3.086937	2.782366	-0.219991
H	-2.325489	2.069529	-1.653003
C	2.150923	-2.421154	-0.286704
H	2.357127	-2.54819	-1.357186
H	2.939872	-2.947148	0.260015
C	0.098883	3.536023	-0.854662
H	1.153197	3.495163	-0.551957
C	-4.882372	-0.921156	-0.120734
H	-5.950448	-1.123366	-0.123946
C	3.678049	0.954976	1.972102
H	4.378713	1.355941	1.234497
H	4.193089	0.940538	2.939774
H	2.836179	1.648682	2.057314
C	3.308324	0.008989	-1.383119
H	2.772362	-0.404577	-2.246707
C	-4.410262	0.383497	-0.293825
H	-5.098187	1.209739	-0.448476
C	2.463216	-1.120419	2.796684
H	1.572977	-0.545288	3.070758

H	3.123865	-1.160562	3.6706
H	2.144298	-2.145986	2.578157
C	4.723617	-0.594319	-1.322715
H	5.315708	-0.173713	-0.50227
H	5.251166	-0.362805	-2.255289
H	4.719785	-1.684966	-1.217267
C	-0.966253	2.834267	1.846594
H	-1.455271	3.798785	1.662344
C	0.01926	3.292684	-2.375046
H	0.25759	2.263805	-2.658463
H	0.71638	3.969506	-2.882498
H	-0.982873	3.52285	-2.756188
C	-0.454402	4.930812	-0.502888
H	-1.534954	4.998489	-0.678519
H	0.022522	5.671833	-1.154927
H	-0.251702	5.22884	0.529786
C	3.343156	1.533603	-1.570051
H	2.335892	1.932984	-1.697818
H	3.908975	1.76806	-2.479295
H	3.830898	2.051692	-0.737953
C	0.360532	3.087868	2.580895
H	0.846157	2.140652	2.836313
H	0.16772	3.623509	3.51758
H	1.063577	3.691064	1.995264
C	-1.915103	1.982242	2.705763
H	-2.904459	1.864485	2.250932
H	-2.059615	2.473966	3.675088
H	-1.502302	0.98572	2.893225
H	-0.113562	-0.131356	1.575039

Table S5 Cartesian coordinates of **2**

angstrom

Atom	x	y	z
C	1.649408	-3.227201	-0.887328
C	1.792701	-4.615068	-0.974606
H	2.745475	-5.058805	-1.24243
C	0.681981	-5.427435	-0.71992
H	0.77302	-6.509078	-0.778979
C	-0.548149	-4.839103	-0.410455
H	-1.430423	-5.449114	-0.239044

C	-0.643895	-3.441919	-0.340627
C	2.724773	-2.251571	-1.18888
C	4.017775	-2.598591	-1.591067
H	4.314432	-3.638988	-1.668323
C	4.925893	-1.580239	-1.9023
H	5.937613	-1.828429	-2.213021
C	4.517159	-0.24501	-1.832405
H	5.195201	0.560184	-2.100511
C	3.207378	0.053572	-1.430134
C	-1.951596	-2.721329	-0.113815
H	-2.613753	-3.297441	0.539748
H	-2.444293	-2.628332	-1.090127
C	2.651849	1.457997	-1.433645
H	2.323936	1.670499	-2.45844
H	3.422067	2.191448	-1.176095
C	-3.285301	-0.0577	-0.001784
H	-3.163333	0.940775	0.444733
C	-3.412447	0.120499	-1.529218
H	-2.505001	0.566101	-1.943036
H	-3.505488	-0.862737	-2.010665
C	-4.651791	0.960397	-1.886411
H	-4.725519	1.046492	-2.977395
H	-4.52666	1.981705	-1.496187
C	-5.938106	0.350611	-1.30883
H	-6.799056	0.992344	-1.532579
H	-6.13126	-0.61726	-1.793597
C	-5.815354	0.145964	0.208724
H	-6.711701	-0.348415	0.60354
H	-5.751507	1.125144	0.70513
C	-4.572277	-0.686984	0.581869
H	-4.69464	-1.705418	0.186067
H	-4.519347	-0.768983	1.67302
C	-1.820048	-1.099032	2.367378
H	-2.838145	-1.464885	2.55864
C	-0.843281	-2.128757	2.972084
H	0.189371	-1.827627	2.75452
H	-0.99039	-3.117117	2.517736
C	-1.030037	-2.237501	4.49749
H	-2.026693	-2.647737	4.715393
H	-0.30093	-2.950091	4.902822
C	-0.880662	-0.87122	5.186002
H	0.155045	-0.518267	5.071329
H	-1.062678	-0.969107	6.263083
C	-1.841761	0.16359	4.579182
H	-1.684473	1.14742	5.038744

H	-2.87818	-0.126093	4.804136
C	-1.666319	0.275594	3.053009
H	-0.665277	0.670703	2.831873
H	-2.392186	0.995439	2.653099
C	1.763896	2.277744	1.295352
H	0.897129	2.204297	1.968267
C	2.880033	1.371814	1.86388
H	3.751875	1.402393	1.194055
H	2.543994	0.330621	1.90669
C	3.325943	1.835645	3.26243
H	2.488922	1.720896	3.966653
H	4.131613	1.183062	3.621565
C	3.78737	3.300665	3.250977
H	4.700752	3.390174	2.644973
H	4.0498	3.624777	4.26532
C	2.696981	4.212852	2.670382
H	3.056762	5.247155	2.605665
H	1.831752	4.222963	3.348951
C	2.232664	3.750421	1.274376
H	3.065706	3.865136	0.564833
H	1.431468	4.414586	0.935119
C	0.18567	3.0866	-1.109566
H	0.889004	3.928171	-1.033817
C	-0.187943	2.925063	-2.597716
H	0.703885	2.739036	-3.207979
H	-0.830856	2.04955	-2.730881
C	-0.892996	4.192128	-3.1186
H	-1.175233	4.038948	-4.167285
H	-0.189342	5.037484	-3.101305
C	-2.131446	4.546389	-2.280132
H	-2.582635	5.477276	-2.644853
H	-2.889092	3.758708	-2.401721
C	-1.772259	4.682524	-0.791854
H	-2.673233	4.872258	-0.194736
H	-1.11434	5.552567	-0.653183
C	-1.06269	3.422025	-0.263057
H	-1.756918	2.5728	-0.308716
H	-0.798902	3.56451	0.793018
N	0.450817	-2.680142	-0.544661
N	2.363929	-0.942579	-1.08804
P	-1.703496	-0.951974	0.495817
P	1.10924	1.63294	-0.358711
Ir	0.434182	-0.606687	-0.393239
H	0.934299	-0.688225	1.103078
Cl	-0.231865	-0.636742	-2.851167

Table S6 Cartesian coordinates of **3**

angstrom

Atom	x	y	z
C	2.73259	-0.912965	-0.194841
C	3.838519	-1.765946	-0.136787
H	4.83461	-1.343434	-0.167211
C	3.664909	-3.157061	-0.049181
C	4.839911	-4.142262	0.020769
C	2.338754	-3.630495	-0.047842
H	2.130903	-4.695539	-0.012762
C	1.258515	-2.747664	-0.113334
C	2.813781	0.562649	-0.348203
C	3.999821	1.285853	-0.450571
H	4.946312	0.762228	-0.379071
C	3.978105	2.680959	-0.654063
C	5.292872	3.466148	-0.757951
C	2.715674	3.281339	-0.771557
H	2.622896	4.34501	-0.959459
C	1.543204	2.519227	-0.669854
C	-0.175966	-3.213892	-0.219805
H	-0.335372	-4.140714	0.340006
H	-0.373674	-3.425655	-1.278209
C	0.168939	3.105538	-0.900675
H	0.004282	3.124045	-1.984739
H	0.109572	4.137733	-0.541771
C	-2.998976	-2.33942	-0.631709
H	-3.723473	-1.593717	-0.270672
C	-2.886444	-2.182792	-2.162817
H	-2.507733	-1.19197	-2.423918
H	-2.146928	-2.894929	-2.554467
C	-4.237775	-2.453907	-2.847677
H	-4.116554	-2.357906	-3.933643
H	-4.963879	-1.685753	-2.541377
C	-4.787983	-3.843051	-2.490443
H	-5.77345	-3.993519	-2.948217
H	-4.124786	-4.614809	-2.907324
C	-4.883	-4.020484	-0.967414
H	-5.216048	-5.036013	-0.718949
H	-5.64267	-3.333389	-0.567178
C	-3.537695	-3.742547	-0.266571
H	-2.810177	-4.506652	-0.576209
H	-3.676762	-3.849126	0.814876
C	-1.775208	-2.227006	2.074542

H	-2.218225	-3.232415	2.080288
C	-0.515232	-2.278385	2.963212
H	-0.009764	-1.304627	2.940345
H	0.199914	-3.017502	2.579652
C	-0.879362	-2.627138	4.418806
H	-1.28458	-3.648608	4.46025
H	0.030435	-2.624205	5.032162
C	-1.913739	-1.64608	4.994046
H	-1.46359	-0.644623	5.064228
H	-2.188096	-1.940676	6.014338
C	-3.167643	-1.579799	4.107401
H	-3.872581	-0.834563	4.496903
H	-3.686256	-2.548793	4.137972
C	-2.814599	-1.239771	2.647175
H	-2.399376	-0.223553	2.601332
H	-3.729332	-1.240418	2.040457
C	-1.571606	2.782457	1.501844
H	-2.234888	2.048223	1.981875
C	-0.294016	2.89732	2.364341
H	0.403516	3.603866	1.891214
H	0.217533	1.930952	2.420537
C	-0.613209	3.404852	3.782182
H	-1.233809	2.660754	4.30272
H	0.318613	3.493871	4.354878
C	-1.351843	4.751342	3.747307
H	-0.682638	5.523341	3.340037
H	-1.615212	5.067544	4.764014
C	-2.614591	4.65981	2.878334
H	-3.102142	5.639967	2.806202
H	-3.337465	3.983747	3.35756
C	-2.30838	4.140281	1.459092
H	-1.689125	4.882163	0.933037
H	-3.249382	4.061101	0.905625
C	-2.713803	2.445106	-1.23678
H	-2.862298	3.524601	-1.090526
C	-2.543354	2.197698	-2.749924
H	-1.691348	2.763404	-3.145507
H	-2.314249	1.14338	-2.9335
C	-3.815558	2.611543	-3.513949
H	-3.678771	2.395923	-4.580646
H	-3.958949	3.698844	-3.427417
C	-5.065037	1.892224	-2.981315
H	-5.959336	2.241656	-3.51187
H	-4.977182	0.814972	-3.184254
C	-5.228414	2.11392	-1.469173

H	-6.086422	1.545719	-1.087796
H	-5.443737	3.175066	-1.27727
C	-3.959511	1.707104	-0.697125
H	-3.802381	0.6261	-0.807272
H	-4.102843	1.902369	0.373617
N	1.471749	-1.415412	-0.152057
N	1.610888	1.197459	-0.428563
P	-1.409067	-1.868326	0.26445
P	-1.208895	2.023861	-0.19351
Ir	-0.057214	-0.011492	-0.181639
H	0.032369	0.149644	1.386706
Cl	0.027692	-0.277383	-2.717744
C	6.204167	-3.426114	0.012944
C	4.725754	-4.969847	1.325669
C	4.774181	-5.089849	-1.203767
H	7.005348	-4.170028	0.071916
H	6.362843	-2.852438	-0.908079
H	6.321744	-2.753558	0.871303
H	5.55353	-5.685326	1.384621
H	4.771823	-4.324942	2.210907
H	3.792552	-5.541474	1.371441
H	5.607782	-5.800147	-1.167644
H	3.8462	-5.671114	-1.226675
H	4.84507	-4.530348	-2.143426
C	5.055937	4.97275	-0.97638
C	6.096268	3.278975	0.553721
C	6.11292	2.918495	-1.953519
H	6.020606	5.487337	-1.035813
H	4.522376	5.174243	-1.912702
H	4.495495	5.425888	-0.149915
H	7.04218	3.828435	0.49077
H	5.540274	3.660005	1.418131
H	6.33844	2.227737	0.744602
H	7.055433	3.470669	-2.039977
H	6.361975	1.85842	-1.834053
H	5.565247	3.031875	-2.895883

Table S7 Cartesian coordinates of 4

angstrom

Atom	x	y	z
C	-1.928829	0.807701	-0.125706
C	-3.055518	1.630821	-0.08372
H	-4.050798	1.199962	-0.051804
C	-2.908089	3.029049	-0.084027
C	-4.100701	3.929478	-0.041493
C	-1.604049	3.546457	-0.149143
H	-1.447553	4.621015	-0.186722
C	-0.500579	2.686014	-0.198549
C	-1.971532	-0.674564	-0.188032
C	-3.143145	-1.433087	-0.20232
H	-4.112118	-0.949833	-0.133232
C	-3.076511	-2.832237	-0.327015
C	-4.318052	-3.664299	-0.344054
C	-1.805046	-3.413977	-0.458007
H	-1.709621	-4.48942	-0.579459
C	-0.654124	-2.616655	-0.444659
C	0.915826	3.181953	-0.379376
H	1.067699	4.141365	0.12483
H	1.071092	3.343416	-1.453652
C	0.729055	-3.173757	-0.691388
H	0.858729	-3.245189	-1.777996
H	0.831475	-4.18309	-0.281045
C	3.742048	2.358753	-0.853066
H	4.50402	1.660842	-0.47422
C	3.581305	2.104763	-2.366676
H	3.228528	1.087923	-2.553444
H	2.803763	2.766595	-2.7726
C	4.897566	2.377762	-3.116363
H	4.741637	2.211266	-4.189306
H	5.660422	1.654062	-2.791675
C	5.411187	3.803464	-2.864315
H	6.374073	3.957486	-3.36677
H	4.707298	4.52611	-3.301954
C	5.553483	4.077156	-1.359356
H	5.858896	5.116506	-1.184995
H	6.35047	3.441453	-0.946956
C	4.24401	3.798688	-0.593939
H	3.480014	4.517854	-0.922531
H	4.41683	3.976945	0.473101
C	2.628241	2.363895	1.901114

H	3.048419	3.376733	1.833651
C	1.403143	2.439323	2.835567
H	0.919931	1.455469	2.887639
H	0.656673	3.140445	2.440448
C	1.81609	2.878049	4.253305
H	2.198776	3.908476	4.220664
H	0.931481	2.891148	4.902334
C	2.894792	1.953405	4.840554
H	2.470886	0.948619	4.986069
H	3.202526	2.312123	5.830331
C	4.113829	1.861862	3.908624
H	4.850192	1.15456	4.310509
H	4.611311	2.841294	3.86334
C	3.711086	1.431793	2.485578
H	3.316938	0.406606	2.513939
H	4.600969	1.415797	1.843116
C	2.529786	-2.664615	1.632817
H	3.186362	-1.886651	2.049005
C	1.282915	-2.763801	2.541037
H	0.592618	-3.515992	2.132105
H	0.74513	-1.810241	2.557665
C	1.660417	-3.178279	3.974678
H	2.275156	-2.38833	4.430649
H	0.749826	-3.258692	4.581749
C	2.43606	-4.504163	3.993625
H	1.77687	-5.316439	3.65411
H	2.740128	-4.752692	5.017739
C	3.667882	-4.430153	3.079691
H	4.180364	-5.399668	3.048064
H	4.386103	-3.708432	3.495104
C	3.302859	-4.002777	1.643721
H	2.688365	-4.789975	1.18203
H	4.22343	-3.931591	1.05587
C	3.578395	-2.4548	-1.155684
H	3.759808	-3.520701	-0.956336
C	3.354943	-2.294987	-2.673686
H	2.506627	-2.902607	-3.010527
H	3.091955	-1.258478	-2.906533
C	4.613585	-2.717982	-3.4549
H	4.438441	-2.564247	-4.526687
H	4.788254	-3.795048	-3.314769
C	5.859337	-1.940052	-3.001947
H	6.745818	-2.295482	-3.541549
H	5.736806	-0.877908	-3.259282
C	6.075086	-2.075196	-1.486159

H	6.929159	-1.466108	-1.163613
H	6.324171	-3.118691	-1.244775
C	4.820352	-1.65836	-0.696366
H	4.632504	-0.588811	-0.858155
H	5.001527	-1.792276	0.378
N	-0.680845	1.350295	-0.154656
N	-0.756824	-1.282593	-0.276684
P	2.201385	1.896283	0.129729
P	2.094094	-2.015775	-0.090599
Ir	0.884174	-0.01569	-0.158639
H	0.851926	-0.085882	1.418645
Cl	0.703748	0.097898	-2.701206
C	-4.457321	4.568922	1.168167
C	-5.584982	5.403498	1.185574
C	-6.356692	5.630491	0.035759
C	-5.97961	4.985222	-1.152379
C	-4.86543	4.13539	-1.214032
C	-3.663182	4.360546	2.44268
H	-5.867095	5.886701	2.119754
C	-7.546566	6.563508	0.068402
H	-6.566308	5.147915	-2.055258
C	-4.503147	3.472277	-2.52826
H	-4.167776	4.828467	3.29261
H	-3.532688	3.29608	2.672842
H	-2.660208	4.800244	2.371842
H	-8.326808	6.241317	-0.629064
H	-7.984291	6.61971	1.070256
H	-7.250057	7.580779	-0.218955
H	-3.458379	3.657624	-2.804852
H	-4.633398	2.383649	-2.486618
H	-5.135969	3.847859	-3.337089
C	-4.793205	-4.191648	-1.568184
C	-5.965796	-4.961462	-1.561558
C	-6.669151	-5.233757	-0.377878
C	-6.175991	-4.699352	0.822312
C	-5.013186	-3.915545	0.861896
C	-4.081165	-3.929427	-2.880758
H	-6.339455	-5.356595	-2.505015

C	-7.909932	-6.098325	-0.393355
H	-6.708305	-4.897535	1.751369
C	-4.526365	-3.371424	2.190782
H	-4.684694	-4.279447	-3.722816
H	-3.877993	-2.862736	-3.03205
H	-3.116045	-4.44902	-2.930551
H	-8.576115	-5.858483	0.441599
H	-8.470939	-5.975772	-1.325705
H	-7.644228	-7.160161	-0.308148
H	-3.475776	-3.627395	2.374619
H	-4.603904	-2.277843	2.237567
H	-5.119827	-3.777963	3.014464

Table S8 Cartesian coordinates of one-electron-reduced **1**

angstrom

Atom	x	y	z
Ir	-0.024522	-0.164758	-0.032612
P	2.218406	0.492157	0.041826
Cl	0.137903	-0.169193	-2.615921
P	-1.601143	1.560416	0.127011
N	0.792048	-2.069701	-0.046632
N	-1.743541	-1.320565	-0.142802
C	-0.149808	-3.090052	0.069931
C	-1.516989	-2.68775	0.007148
C	0.317862	-4.428448	0.214548
H	-0.397973	-5.236845	0.327943
C	3.092479	0.901764	1.662978
H	4.162426	0.799691	1.434411
C	2.113246	-2.33383	-0.106371
C	-2.987867	-0.82767	-0.321118
C	1.673348	-4.692632	0.206968
H	2.029172	-5.714485	0.31951
C	2.605576	-3.630183	0.031136
H	3.673062	-3.817837	-0.027321
C	-2.644296	-3.558381	0.054117
H	-2.492296	-4.62474	0.19037
C	-3.076486	0.656239	-0.60511

H	-4.034227	1.071122	-0.273531
H	-2.998003	0.795688	-1.690011
C	3.013268	-1.157879	-0.41021
H	3.153467	-1.122791	-1.498014
H	3.99828	-1.281754	0.05185
C	-1.564031	3.219767	-0.778663
H	-0.633402	3.681213	-0.422283
C	-3.919828	-3.047969	-0.084557
H	-4.779017	-3.714401	-0.051618
C	2.838931	2.33778	2.151389
H	3.258378	3.087299	1.473497
H	3.30608	2.481958	3.133849
H	1.768743	2.54027	2.260866
C	2.956605	1.613432	-1.279475
H	2.65599	1.078864	-2.18951
C	-4.110842	-1.650596	-0.289678
H	-5.099979	-1.231129	-0.443708
C	2.73638	-0.125164	2.752443
H	1.67605	-0.064976	3.018597
H	3.329226	0.075017	3.654061
H	2.939045	-1.154892	2.439126
C	4.491496	1.707767	-1.227067
H	4.838746	2.267788	-0.35055
H	4.855688	2.237131	-2.11646
H	4.972307	0.72335	-1.214483
C	-2.20579	2.015557	1.855901
H	-3.094243	2.637335	1.687591
C	-1.452671	3.029468	-2.304097
H	-0.737169	2.24969	-2.582074
H	-1.150581	3.977061	-2.767806
H	-2.423412	2.753689	-2.733858
C	-2.732388	4.165916	-0.440979
H	-3.702752	3.706837	-0.666799
H	-2.651518	5.069075	-1.058809
H	-2.738839	4.485194	0.60572
C	2.300826	3.001103	-1.347032
H	1.217461	2.910346	-1.442512
H	2.669927	3.534937	-2.231811
H	2.527982	3.618808	-0.471133
C	-1.161578	2.844926	2.620866
H	-0.280735	2.234403	2.844292
H	-1.580223	3.186398	3.575827
H	-0.832526	3.73155	2.066174
C	-2.639912	0.791705	2.680181
H	-3.442351	0.225383	2.197024

H	-3.008375	1.126659	3.658484
H	-1.802079	0.107527	2.847217
H	-0.072134	-0.25374	1.541601

Table S9 Cartesian coordinates of one-electron-reduced **2**

angstrom

Atom	x	y	z
C	1.634667	-3.181048	-0.994225
C	1.757658	-4.599456	-1.060493
H	2.716884	-5.043526	-1.30865
C	0.659956	-5.401628	-0.817127
H	0.755639	-6.484065	-0.869441
C	-0.602263	-4.8139	-0.514223
H	-1.487139	-5.422828	-0.358222
C	-0.686729	-3.424399	-0.455237
C	2.672838	-2.239963	-1.268273
C	4.007851	-2.560403	-1.650782
H	4.310723	-3.600716	-1.720676
C	4.907028	-1.551627	-1.936522
H	5.925474	-1.798203	-2.228999
C	4.498268	-0.188487	-1.867396
H	5.174755	0.61896	-2.129329
C	3.186821	0.089699	-1.487964
C	-1.997992	-2.702087	-0.224506
H	-2.675182	-3.293215	0.400802
H	-2.476665	-2.556649	-1.200888
C	2.62799	1.497736	-1.479428
H	2.252592	1.708001	-2.487559
H	3.401987	2.236802	-1.247535
C	-3.31074	-0.0412	0.058801
H	-3.170609	0.933823	0.550839
C	-3.476491	0.217911	-1.45288
H	-2.572206	0.668909	-1.868115
H	-3.590906	-0.73888	-1.980336
C	-4.713319	1.087509	-1.73749
H	-4.813236	1.233085	-2.820744
H	-4.569467	2.08576	-1.296044
C	-5.993075	0.460801	-1.16191
H	-6.855296	1.118849	-1.332926
H	-6.202962	-0.481035	-1.689837

C	-5.83588	0.175582	0.340094
H	-6.730129	-0.328266	0.73061
H	-5.74886	1.128889	0.882398
C	-4.591403	-0.684737	0.637637
H	-4.731324	-1.680563	0.193421
H	-4.512703	-0.82591	1.721503
C	-1.80374	-1.200512	2.323547
H	-2.819317	-1.567133	2.528984
C	-0.819122	-2.263575	2.853457
H	0.207296	-1.964026	2.608993
H	-0.989097	-3.227724	2.359662
C	-0.952445	-2.43482	4.377834
H	-1.94648	-2.842206	4.616398
H	-0.217667	-3.171624	4.727451
C	-0.76195	-1.100594	5.117886
H	0.271432	-0.752189	4.972526
H	-0.900641	-1.239772	6.198103
C	-1.734797	-0.032942	4.590707
H	-1.551557	0.929633	5.086563
H	-2.764798	-0.326384	4.842445
C	-1.614995	0.139419	3.065089
H	-0.620811	0.537743	2.821053
H	-2.348734	0.881331	2.72285
C	1.849756	2.198054	1.31442
H	1.005626	2.102957	2.013898
C	2.966846	1.244505	1.796183
H	3.813462	1.289767	1.097062
H	2.610116	0.210221	1.790083
C	3.468414	1.622253	3.200669
H	2.653319	1.487507	3.927626
H	4.272538	0.93637	3.497399
C	3.96033	3.07698	3.252214
H	4.850842	3.180261	2.614731
H	4.268225	3.342863	4.271972
C	2.868781	4.039484	2.760023
H	3.246432	5.070462	2.74132
H	2.027911	4.024746	3.469312
C	2.346718	3.659733	1.359593
H	3.155952	3.797069	0.626989
H	1.547806	4.356656	1.084851
C	0.208024	3.154373	-0.971235
H	0.91439	3.990699	-0.867818
C	-0.211072	3.080551	-2.453948
H	0.667324	2.947833	-3.096128
H	-0.836975	2.198401	-2.622584

C	-0.952433	4.361144	-2.881129
H	-1.267176	4.263197	-3.927992
H	-0.262894	5.218159	-2.836689
C	-2.168417	4.648111	-1.985506
H	-2.651685	5.587239	-2.285909
H	-2.912619	3.849903	-2.120767
C	-1.758194	4.712687	-0.505338
H	-2.640742	4.860085	0.131618
H	-1.105985	5.584609	-0.34741
C	-1.013986	3.437229	-0.070173
H	-1.698728	2.581359	-0.131154
H	-0.713401	3.52867	0.982055
N	0.39478	-2.643156	-0.654338
N	2.322134	-0.89506	-1.167143
P	-1.714218	-0.971202	0.454162
P	1.131265	1.635479	-0.348478
Ir	0.407153	-0.582261	-0.445166
H	0.957355	-0.761136	1.020661
Cl	-0.352022	-0.449507	-2.90881

Table S10 Cartesian coordinates of one-electron-reduced **3**

angstrom

Atom	x	y	z
C	2.690627	-0.958655	-0.288836
C	3.778312	-1.877448	-0.201113
H	4.78519	-1.477588	-0.212447
C	3.568706	-3.242186	-0.110027
C	4.712265	-4.262386	-0.016581
C	2.211051	-3.706584	-0.119955
H	1.976376	-4.76547	-0.090417
C	1.168665	-2.791234	-0.204705
C	2.803941	0.458616	-0.433364
C	4.01725	1.197617	-0.516616
H	4.952879	0.654208	-0.430208
C	4.023742	2.571936	-0.710267
C	5.3576	3.337429	-0.795992
C	2.760904	3.226549	-0.839909
H	2.690945	4.289993	-1.032786
C	1.585502	2.482158	-0.751257
C	-0.280977	-3.222002	-0.308494

H	-0.459625	-4.160004	0.227826
H	-0.507365	-3.388997	-1.368702
C	0.220725	3.100891	-0.978797
H	0.02229	3.072353	-2.05645
H	0.193678	4.147975	-0.65927
C	-3.099759	-2.271549	-0.561571
H	-3.777621	-1.493781	-0.177046
C	-3.054589	-2.132571	-2.09761
H	-2.637123	-1.16504	-2.386495
H	-2.36741	-2.881957	-2.514159
C	-4.445806	-2.346966	-2.718243
H	-4.373443	-2.261698	-3.810093
H	-5.124432	-1.547522	-2.382967
C	-5.037817	-3.709932	-2.326196
H	-6.049083	-3.824521	-2.738518
H	-4.42352	-4.509851	-2.765134
C	-5.068475	-3.874994	-0.79851
H	-5.434393	-4.874478	-0.527793
H	-5.779651	-3.152469	-0.371072
C	-3.682107	-3.646702	-0.163096
H	-3.000033	-4.441991	-0.496615
H	-3.775412	-3.740449	0.924681
C	-1.740593	-2.223553	2.065722
H	-2.206273	-3.218884	2.089832
C	-0.439116	-2.310373	2.889594
H	0.090333	-1.351201	2.837841
H	0.236558	-3.062646	2.465506
C	-0.734615	-2.652523	4.361409
H	-1.165332	-3.663225	4.424777
H	0.206128	-2.67483	4.926783
C	-1.711125	-1.646414	4.99272
H	-1.232314	-0.656698	5.03322
H	-1.937499	-1.931872	6.028489
C	-3.00856	-1.547444	4.173401
H	-3.673958	-0.785851	4.601525
H	-3.546808	-2.50522	4.231692
C	-2.723213	-1.215327	2.696937
H	-2.286421	-0.209691	2.628146
H	-3.668706	-1.190833	2.138926
C	-1.381028	2.838301	1.524435
H	-2.047409	2.131452	2.041365
C	-0.051002	2.887888	2.310187
H	0.651439	3.560282	1.798129
H	0.416143	1.898718	2.325001
C	-0.259936	3.395357	3.747316

H	-0.884952	2.677851	4.300086
H	0.707501	3.43494	4.26479
C	-0.933244	4.776311	3.766606
H	-0.253193	5.516321	3.319291
H	-1.118237	5.099696	4.799404
C	-2.249607	4.752207	2.974653
H	-2.694783	5.755487	2.940037
H	-2.971565	4.104938	3.494462
C	-2.054406	4.228204	1.537523
H	-1.434441	4.943814	0.977219
H	-3.030632	4.198096	1.041908
C	-2.705096	2.557384	-1.120082
H	-2.820705	3.638658	-0.95699
C	-2.639359	2.31978	-2.642806
H	-1.810521	2.884641	-3.085126
H	-2.422088	1.2665	-2.847538
C	-3.953666	2.743882	-3.324391
H	-3.887601	2.531025	-4.399079
H	-4.086456	3.832177	-3.224543
C	-5.172247	2.031507	-2.715675
H	-6.097795	2.381737	-3.191609
H	-5.09811	0.953218	-2.918825
C	-5.238608	2.257117	-1.196466
H	-6.078149	1.698202	-0.761546
H	-5.430751	3.321785	-0.996014
C	-3.927213	1.839657	-0.506694
H	-3.788389	0.756546	-0.620234
H	-3.999719	2.038805	0.570733
N	1.394672	-1.46301	-0.255419
N	1.602631	1.156864	-0.521473
P	-1.442285	-1.847882	0.242091
P	-1.141171	2.067278	-0.192152
Ir	-0.078529	-0.012051	-0.234601
H	0.118456	0.124167	1.322359
Cl	-0.175558	-0.242463	-2.807481
C	6.101004	-3.594758	-0.015569
C	4.566959	-5.077004	1.293063
C	4.640317	-5.225038	-1.228392
H	6.88	-4.362807	0.057797
H	6.280602	-3.029293	-0.937498
H	6.224967	-2.914978	0.835821
H	5.366208	-5.825305	1.367523
H	4.629479	-4.421075	2.169451

H	3.60865	-5.605221	1.339557
H	5.446577	-5.967547	-1.173498
H	3.688948	-5.766358	-1.263383
H	4.744284	-4.674249	-2.170338
C	5.152659	4.850167	-1.012852
C	6.149778	3.143777	0.520497
C	6.191401	2.790922	-1.981157
H	6.127081	5.350613	-1.059584
H	4.628729	5.059779	-1.95272
H	4.585009	5.30657	-0.193273
H	7.10518	3.682252	0.474644
H	5.582886	3.525418	1.377939
H	6.369019	2.087742	0.710322
H	7.143684	3.331212	-2.059717
H	6.418618	1.72645	-1.860763
H	5.650539	2.909772	-2.927099

Table S11 Cartesian coordinates of one-electron-reduced 4

angstrom

Atom	x	y	z
C	-1.928829	0.807701	-0.125706
C	-3.055518	1.630821	-0.08372
H	-4.050798	1.199962	-0.051804
C	-2.908089	3.029049	-0.084027
C	-4.100701	3.929478	-0.041493
C	-1.604049	3.546457	-0.149143
H	-1.447553	4.621015	-0.186722
C	-0.500579	2.686014	-0.198549
C	-1.971532	-0.674564	-0.188032
C	-3.143145	-1.433087	-0.20232
H	-4.112118	-0.949833	-0.133232
C	-3.076511	-2.832237	-0.327015
C	-4.318052	-3.664299	-0.344054
C	-1.805046	-3.413977	-0.458007
H	-1.709621	-4.48942	-0.579459
C	-0.654124	-2.616655	-0.444659

C	0.915826	3.181953	-0.379376
H	1.067699	4.141365	0.12483
H	1.071092	3.343416	-1.453652
C	0.729055	-3.173757	-0.691388
H	0.858729	-3.245189	-1.777996
H	0.831475	-4.18309	-0.281045
C	3.742048	2.358753	-0.853066
H	4.50402	1.660842	-0.47422
C	3.581305	2.104763	-2.366676
H	3.228528	1.087923	-2.553444
H	2.803763	2.766595	-2.7726
C	4.897566	2.377762	-3.116363
H	4.741637	2.211266	-4.189306
H	5.660422	1.654062	-2.791675
C	5.411187	3.803464	-2.864315
H	6.374073	3.957486	-3.36677
H	4.707298	4.52611	-3.301954
C	5.553483	4.077156	-1.359356
H	5.858896	5.116506	-1.184995
H	6.35047	3.441453	-0.946956
C	4.24401	3.798688	-0.593939
H	3.480014	4.517854	-0.922531
H	4.41683	3.976945	0.473101
C	2.628241	2.363895	1.901114
H	3.048419	3.376733	1.833651
C	1.403143	2.439323	2.835567
H	0.919931	1.455469	2.887639
H	0.656673	3.140445	2.440448
C	1.81609	2.878049	4.253305
H	2.198776	3.908476	4.220664
H	0.931481	2.891148	4.902334
C	2.894792	1.953405	4.840554
H	2.470886	0.948619	4.986069
H	3.202526	2.312123	5.830331
C	4.113829	1.861862	3.908624
H	4.850192	1.15456	4.310509
H	4.611311	2.841294	3.86334
C	3.711086	1.431793	2.485578
H	3.316938	0.406606	2.513939
H	4.600969	1.415797	1.843116
C	2.529786	-2.664615	1.632817
H	3.186362	-1.886651	2.049005
C	1.282915	-2.763801	2.541037
H	0.592618	-3.515992	2.132105
H	0.74513	-1.810241	2.557665

C	1.660417	-3.178279	3.974678
H	2.275156	-2.38833	4.430649
H	0.749826	-3.258692	4.581749
C	2.43606	-4.504163	3.993625
H	1.77687	-5.316439	3.65411
H	2.740128	-4.752692	5.017739
C	3.667882	-4.430153	3.079691
H	4.180364	-5.399668	3.048064
H	4.386103	-3.708432	3.495104
C	3.302859	-4.002777	1.643721
H	2.688365	-4.789975	1.18203
H	4.22343	-3.931591	1.05587
C	3.578395	-2.4548	-1.155684
H	3.759808	-3.520701	-0.956336
C	3.354943	-2.294987	-2.673686
H	2.506627	-2.902607	-3.010527
H	3.091955	-1.258478	-2.906533
C	4.613585	-2.717982	-3.4549
H	4.438441	-2.564247	-4.526687
H	4.788254	-3.795048	-3.314769
C	5.859337	-1.940052	-3.001947
H	6.745818	-2.295482	-3.541549
H	5.736806	-0.877908	-3.259282
C	6.075086	-2.075196	-1.486159
H	6.929159	-1.466108	-1.163613
H	6.324171	-3.118691	-1.244775
C	4.820352	-1.65836	-0.696366
H	4.632504	-0.588811	-0.858155
H	5.001527	-1.792276	0.378
N	-0.680845	1.350295	-0.154656
N	-0.756824	-1.282593	-0.276684
P	2.201385	1.896283	0.129729
P	2.094094	-2.015775	-0.090599
Ir	0.884174	-0.01569	-0.158639
H	0.851926	-0.085882	1.418645
Cl	0.703748	0.097898	-2.701206
C	-4.457321	4.568922	1.168167
C	-5.584982	5.403498	1.185574
C	-6.356692	5.630491	0.035759
C	-5.97961	4.985222	-1.152379
C	-4.86543	4.13539	-1.214032
C	-3.663182	4.360546	2.44268
H	-5.867095	5.886701	2.119754

C	-7.546566	6.563508	0.068402
H	-6.566308	5.147915	-2.055258
C	-4.503147	3.472277	-2.52826
H	-4.167776	4.828467	3.29261
H	-3.532688	3.29608	2.672842
H	-2.660208	4.800244	2.371842
H	-8.326808	6.241317	-0.629064
H	-7.984291	6.61971	1.070256
H	-7.250057	7.580779	-0.218955
H	-3.458379	3.657624	-2.804852
H	-4.633398	2.383649	-2.486618
H	-5.135969	3.847859	-3.337089
C	-4.793205	-4.191648	-1.568184
C	-5.965796	-4.961462	-1.561558
C	-6.669151	-5.233757	-0.377878
C	-6.175991	-4.699352	0.822312
C	-5.013186	-3.915545	0.861896
C	-4.081165	-3.929427	-2.880758
H	-6.339455	-5.356595	-2.505015
C	-7.909932	-6.098325	-0.393355
H	-6.708305	-4.897535	1.751369
C	-4.526365	-3.371424	2.190782
H	-4.684694	-4.279447	-3.722816
H	-3.877993	-2.862736	-3.03205
H	-3.116045	-4.44902	-2.930551
H	-8.576115	-5.858483	0.441599
H	-8.470939	-5.975772	-1.325705
H	-7.644228	-7.160161	-0.308148
H	-3.475776	-3.627395	2.374619
H	-4.603904	-2.277843	2.237567
H	-5.119827	-3.777963	3.014464

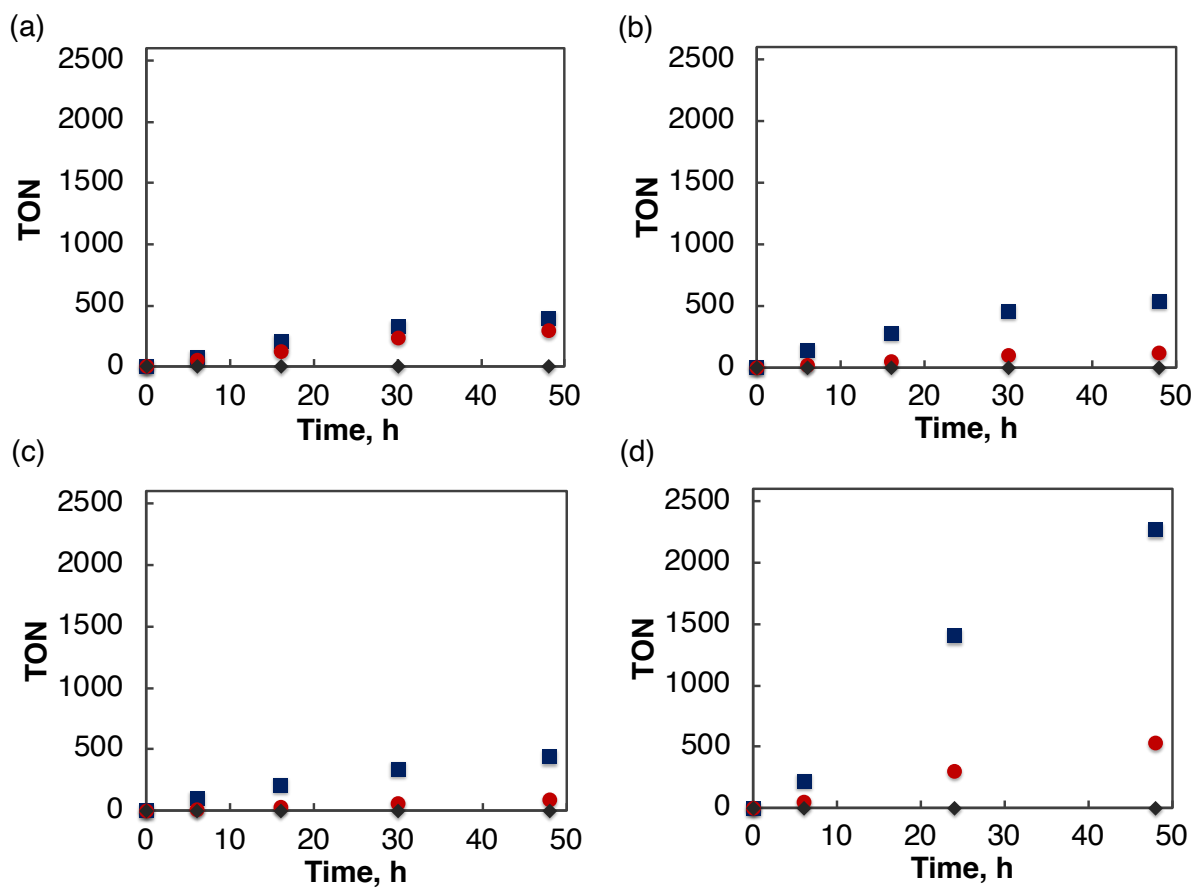


Fig. S1 Time course plots of products [HCO₂H (blue), CO (red) and H₂ (black)] obtained in the photocatalytic CO₂ reduction with a catalytic amount of (a) **1**, (b) **2**, (c) **3** and (d) **4** (20 μ M) in a CO₂-saturated mixture of DMA:H₂O (9:1, v/v) and BIH (0.2 M) under photoirradiation ($\lambda \geq 400$ nm) at 298 K.

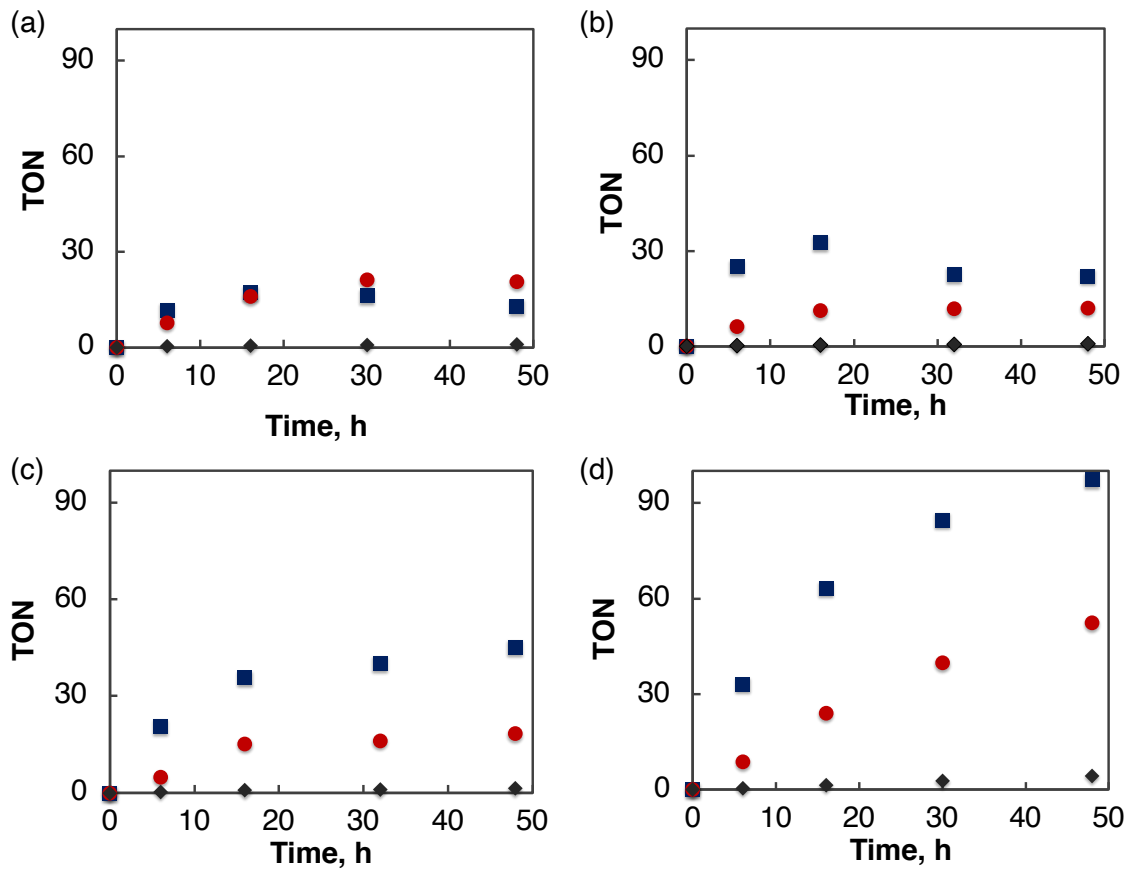


Fig. S2 Time course plots of products [HCO_2H (blue), CO (red) and H_2 (black)] obtained in the photocatalytic CO_2 reduction with a catalytic amount of (a) 1, (b) 2, (c) 3 and (d) 4 (0.10 mM) under a CO_2 atmosphere in a mixture of DMA/ H_2O /TEOA (9:1:2, v/v/v) under photoirradiation ($\lambda \geq 400$ nm) at 298 K.

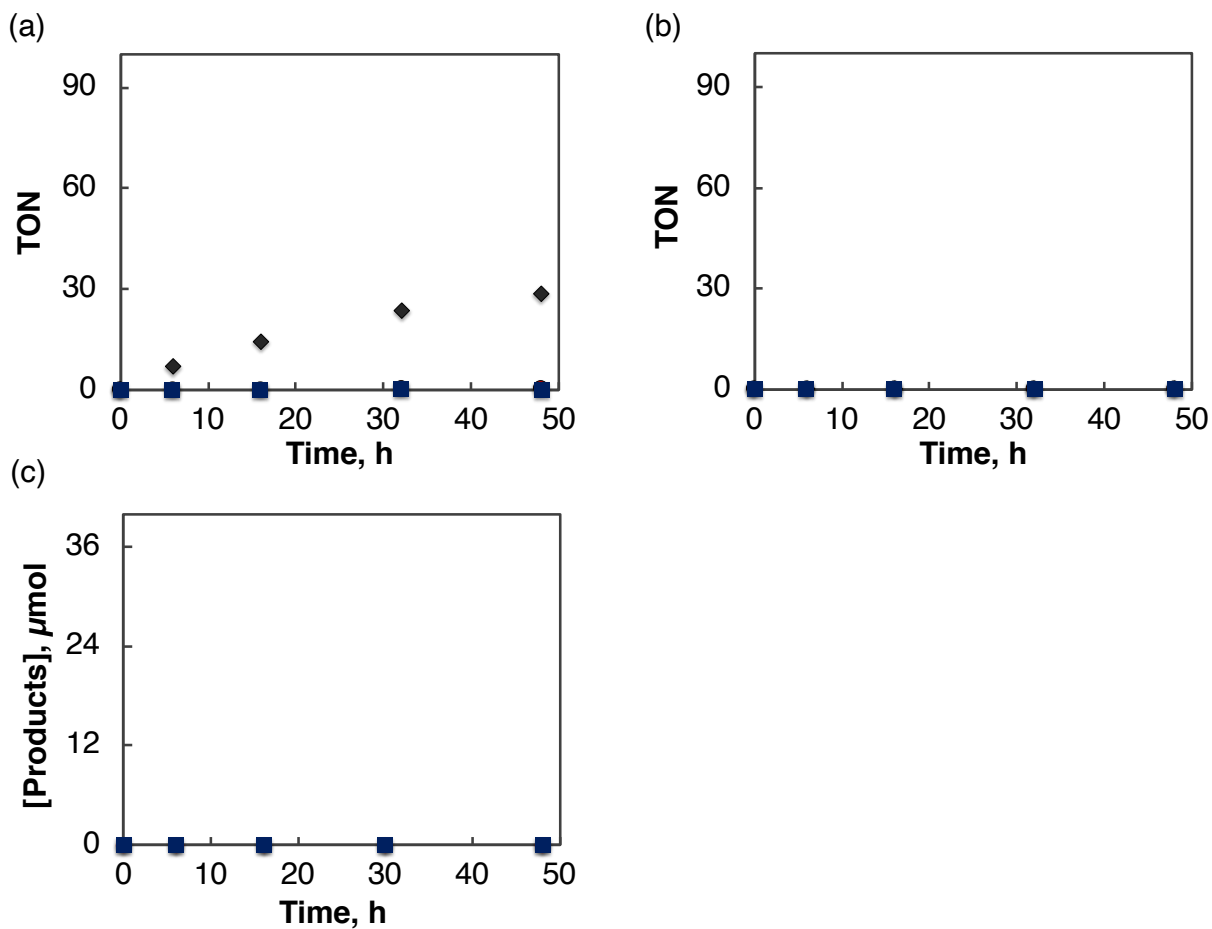


Fig. S3 Time course plots of products [HCO_2H (blue), CO (red) and H_2 (black)] produced in the photocatalytic CO_2 reduction in a mixture solution of DMA/ H_2O /TEOA (9:1:2, v/v/v; 4.0 mL) containing **4** (0.1 mM) upon photoirradiation ($\lambda \geq 400$ nm) (a) under an Ar atmosphere; (b) under a CO_2 atmosphere without TEOA and (c) under a CO_2 atmosphere without **4**.

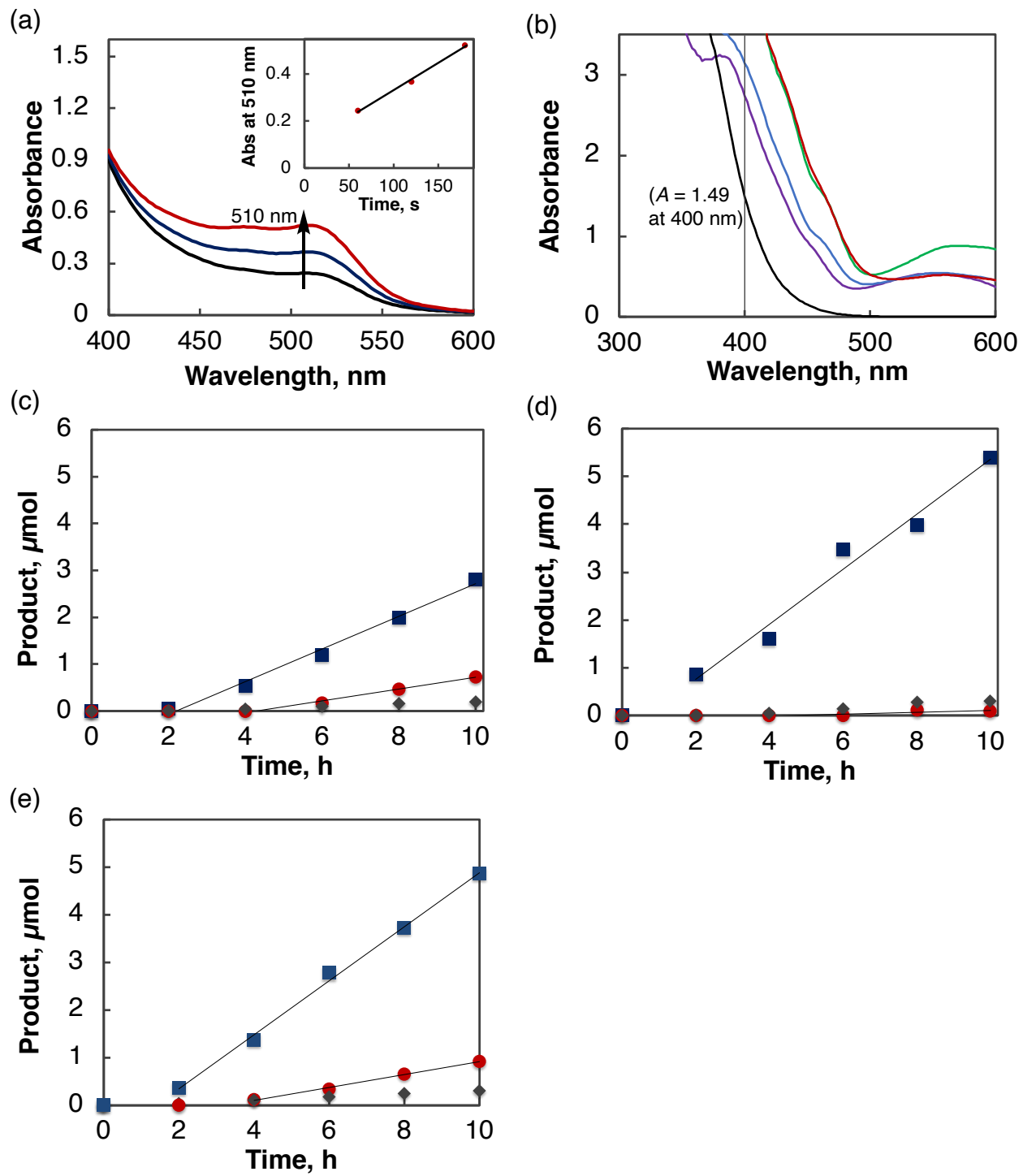


Fig. S4 (a) UV-vis absorption spectral change of $[\text{Fe}(\text{phen})_3]^{2+}$ formed by the reaction of phenanthroline with Fe^{2+} ion, which was produced by photoirradiation of ferrioxalate actinometer using monochromatized light ($\lambda = 400 \text{ nm}$) for 1, 2, and 3 min at 298 K. (b) UV-vis absorption spectral change of ferrioxalate actinometer [6.0 mM, $\text{Abs} = 1.49$, percentage of light absorption = $(1 - 10^{-1.49}) \times 100 =$

96.8%; black line] using monochromatized light ($\lambda = 400$ nm) for 3 min and the reaction solution [Abs > 2, percentage of light absorption > 99%] obtained in the photocatalytic CO₂ reduction by the Ir complexes [IrPCY2 (**2**, blue), *t*Bu-IrPCY2 (**3**, green) and Mes-IrPCY2 (**4**, red); 1.5 mM] under photoirradiation for 5 h with monochromatized light ($\lambda = 400$ nm) in CO₂-saturated mixture of DMA/H₂O/TEOA (9:1:2, v/v/v; 2.0 mL) at 298 K. Time courses of formation of HCO₂H (blue) and CO (red) produced in the photocatalytic reduction of CO₂ in a CO₂-saturated mixture of DMA/H₂O/TEOA (9:1:2, v/v/v; 4.0 mL) containing (c) **2**, (d) **3** or (e) **4** (1.5 mM) under photoirradiation with monochromatized light ($\lambda_{\text{ex}} = 400$ nm) for 10 h.

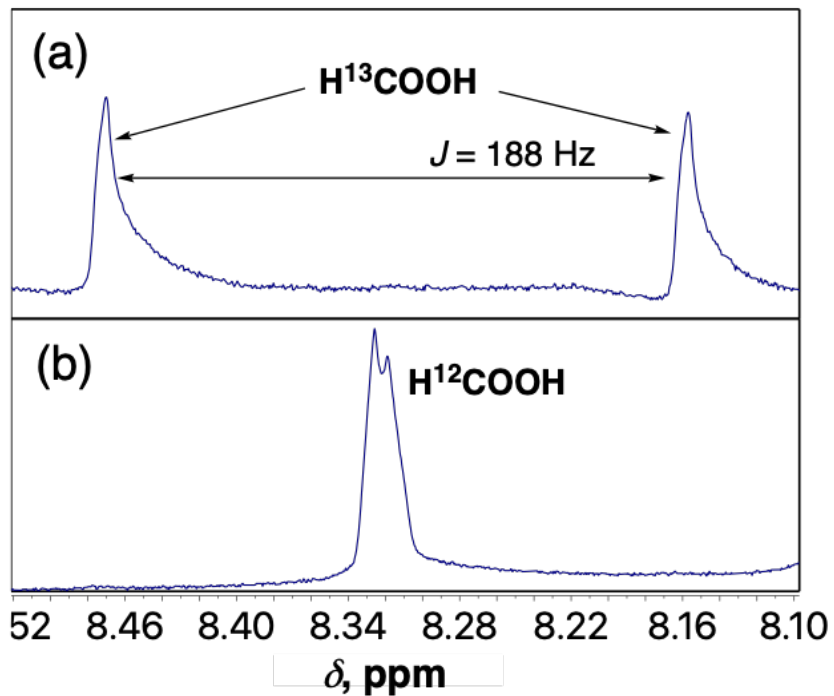


Fig. S5 ¹H NMR spectra of the reaction solution after 20 h of irradiation ($\lambda > 400 \text{ nm}$) of DMA-*d*₉/TEOA/H₂O (9:2:1, v/v/v) solutions containing **4** (1.0 mM) under (a) ¹³CO₂ or (b) unlabeled CO₂.

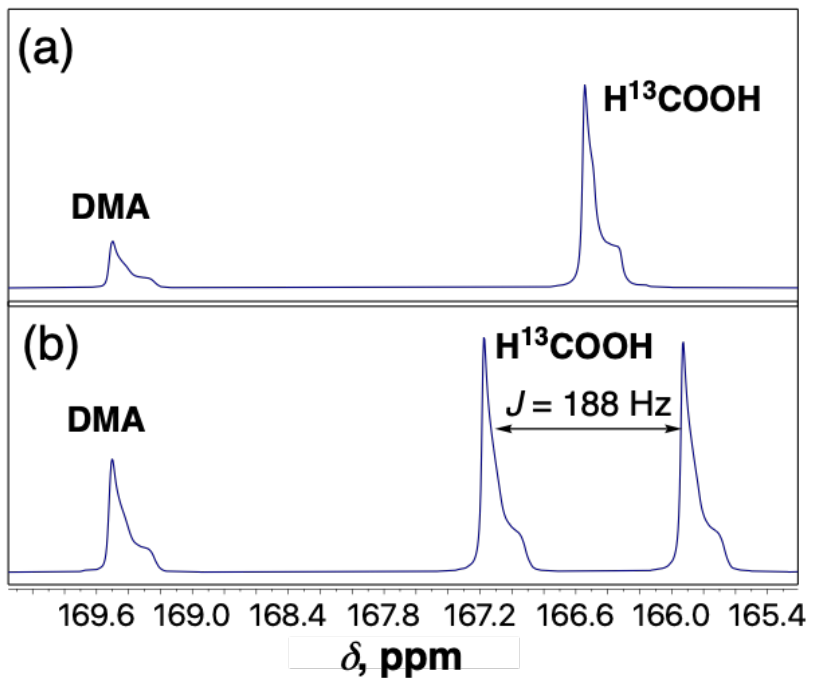


Fig. S6 ^{13}C NMR spectrum of the photocatalytic reaction solution (a) with proton-decoupling and (b) without decoupling after 20 h of irradiation ($\lambda \geq 400 \text{ nm}$) of DMA- $d_9/\text{H}_2\text{O}/\text{TEOA}$ (9:1:2, v/v/v) solutions containing **4** (1.0 mM) under a $^{13}\text{CO}_2$ atmosphere. Chemical shifts are internally referenced to DMA (169.5 ppm).^{S6}

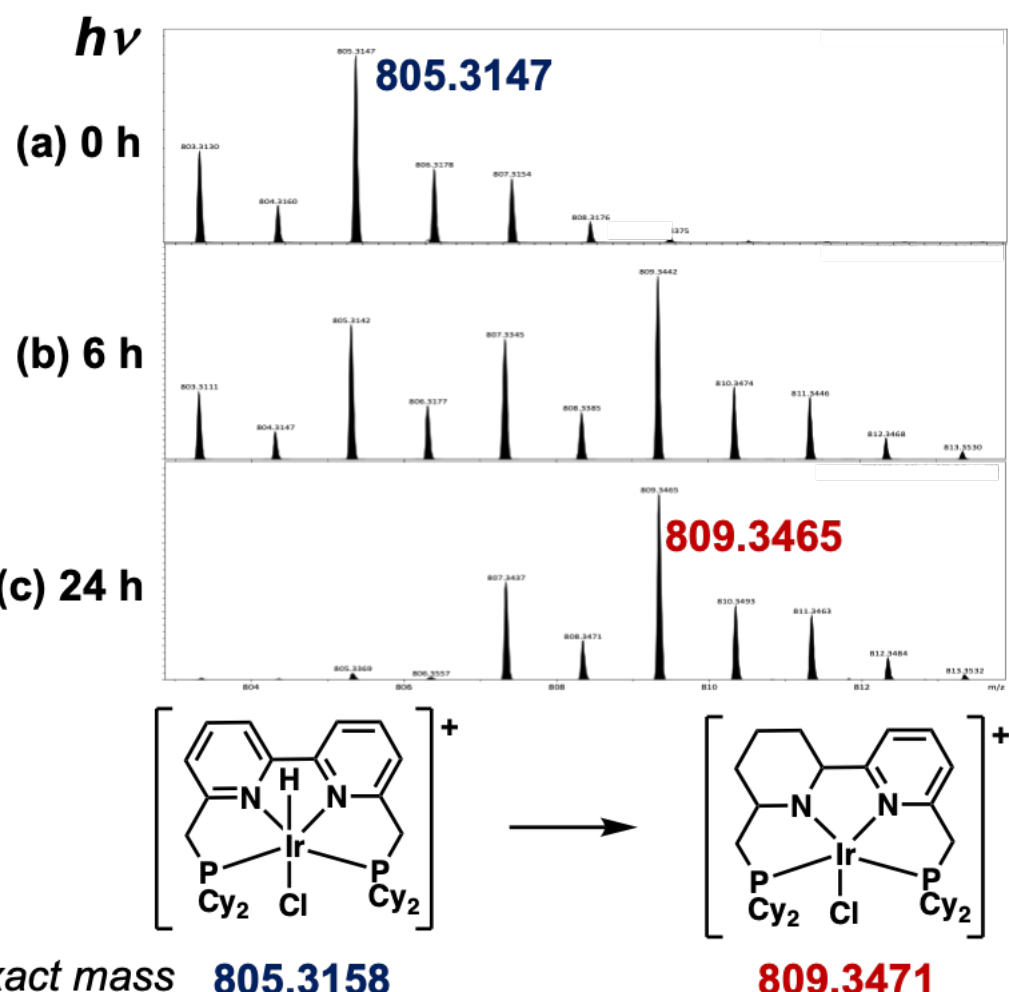


Fig. S7 ESI-MS measurements of a CO₂-saturated mixture of CH₃CN/TEOA (5:1, v/v; 4.0 mL) containing 0.1 mM of **2** after extraction with CH₂Cl₂ (a) before photoirradiation and after photoirradiation ($\lambda \geq 400$ nm) in (b) 6 h and (c) 24 h.

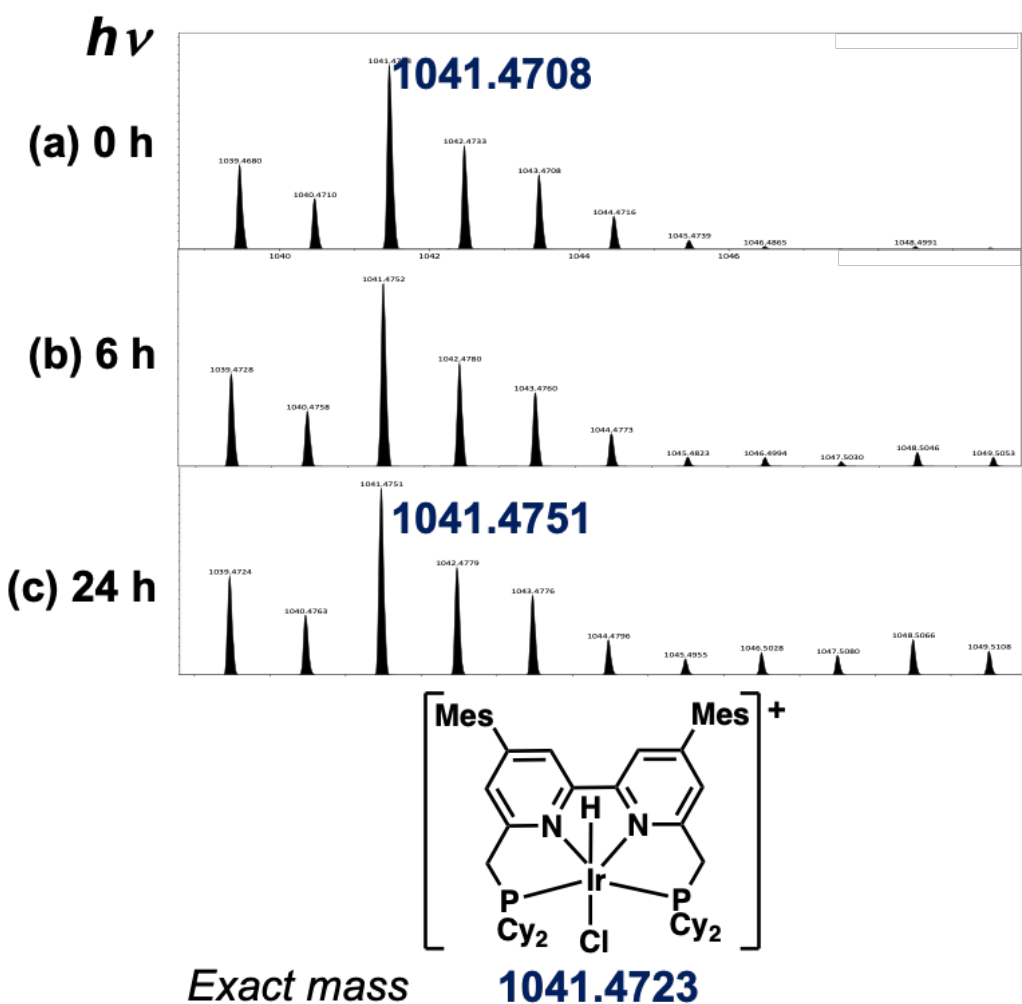


Fig. S8 ESI-MS measurements of a CO₂-saturated mixture of CH₃CN/TEOA (5:1, v/v; 4.0 mL) containing 0.1 mM of **4** after extraction with CH₂Cl₂ (a) before photoirradiation and after photoirradiation ($\lambda \geq 400$ nm) in (b) 6 h and (c) 24 h.

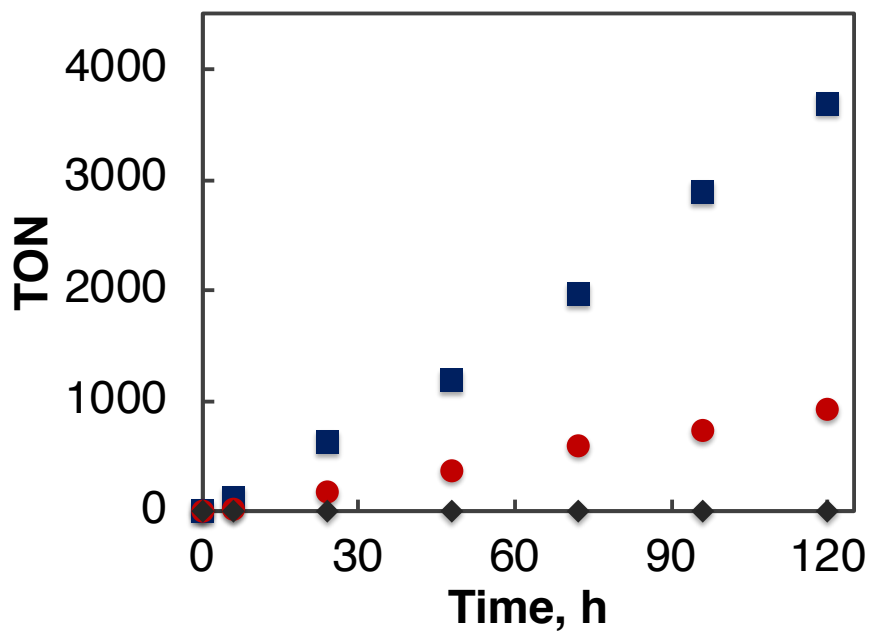


Fig. S9 Time course plots of products [HCO₂H (blue), CO (red) and H₂ (black)] produced in photo-catalytic reduction of CO₂ in a mixture solution of DMA/H₂O (9:1, v/v; 4 mL) containing **4** (20 μ M) and BIH (0.25 M) under solar simulator light under a CO₂ atmosphere. The reaction vessel was scaled up with a bigger size of test tube where the volume of a reaction vessel was changed from 8 mL to 35 mL.

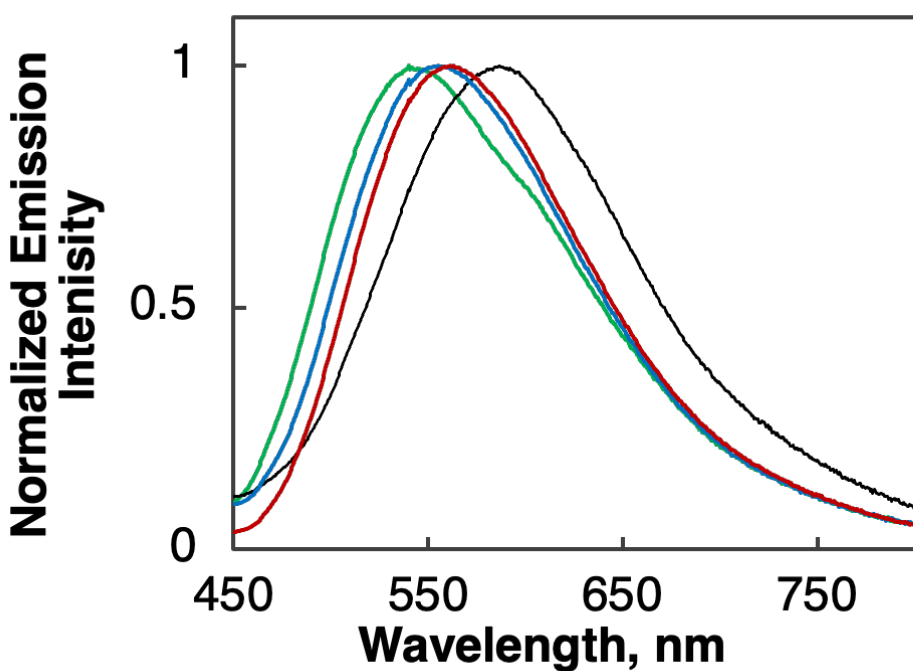


Fig. S10 Fluorescence emission spectra of the 0.1 mM of Ir complexes [1 (black), 2 (blue), 3 (green) and 4 (red)] in a deaerated DMA solution. Excitation wavelength: 380 nm.

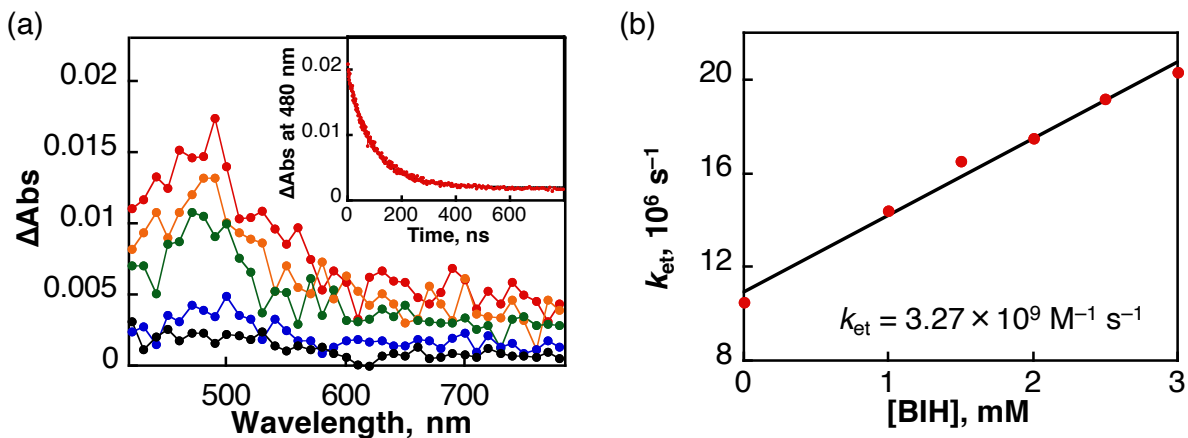


Fig. S11 (a) Transient absorption spectral changes [red (2 ns); orange (20 ns); green (50 ns); blue (200 ns); black (500 ns)] after sub-nanosecond laser excitation at 355 nm in a deaerated DMA solution containing **1** (2.0 mM) at 298 K. Inset shows the decay time profile of the absorbance at 480 nm due to the decay of the excited state of **1**. (b) Plot of k_{obs} vs concentration of BIH in a DMA solution at 298 K.

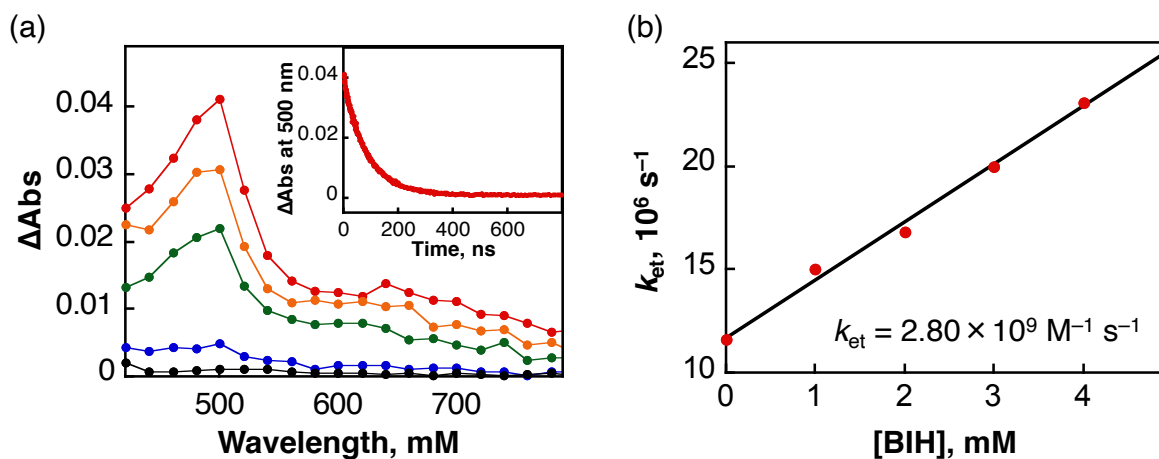


Fig. S12 (a) Transient absorption spectral changes [red (2 ns); orange (20 ns); green (50 ns); blue (200 ns); black (500 ns)] after sub-nanosecond laser excitation at 355 nm in a deaerated DMA solution containing **3** (1.5 mM) at 298 K. Inset shows the decay time profile of the absorbance at 500 nm due to the decay of the excited state of **3**. (b) Plot of k_{obs} vs concentration of BIH in a DMA solution at 298 K.

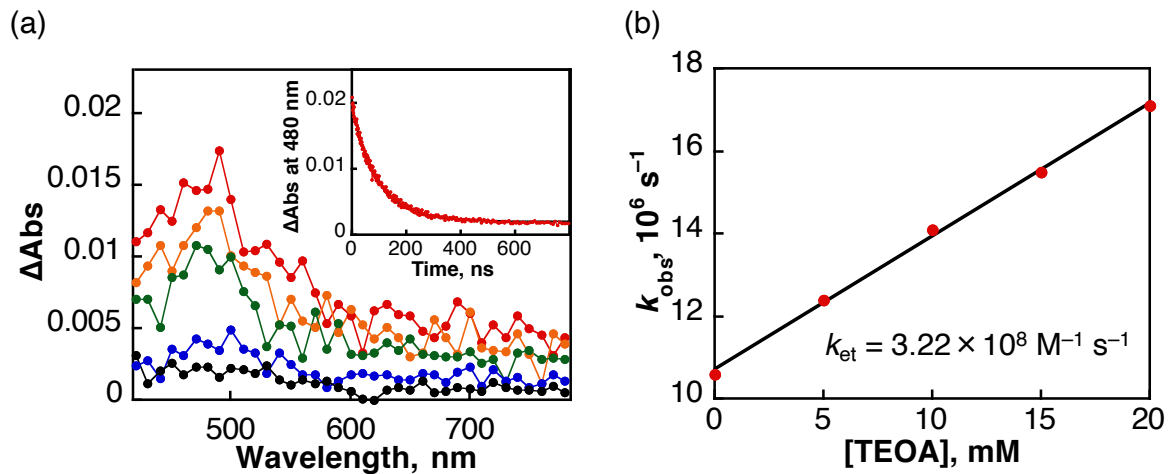


Fig. S13 (a) Transient absorption spectral changes [red (2 ns); orange (20 ns); green (50 ns); blue (200 ns); black (500 ns)] after sub-nanosecond laser excitation at 355 nm in a deaerated DMA solution containing **1** (2.0 mM) at 298 K. Inset shows the decay time profile of the absorbance at 480 nm due to the decay of the excited state of **1**. (b) Plot of k_{obs} vs concentration of TEOA in a DMA solution at 298 K.

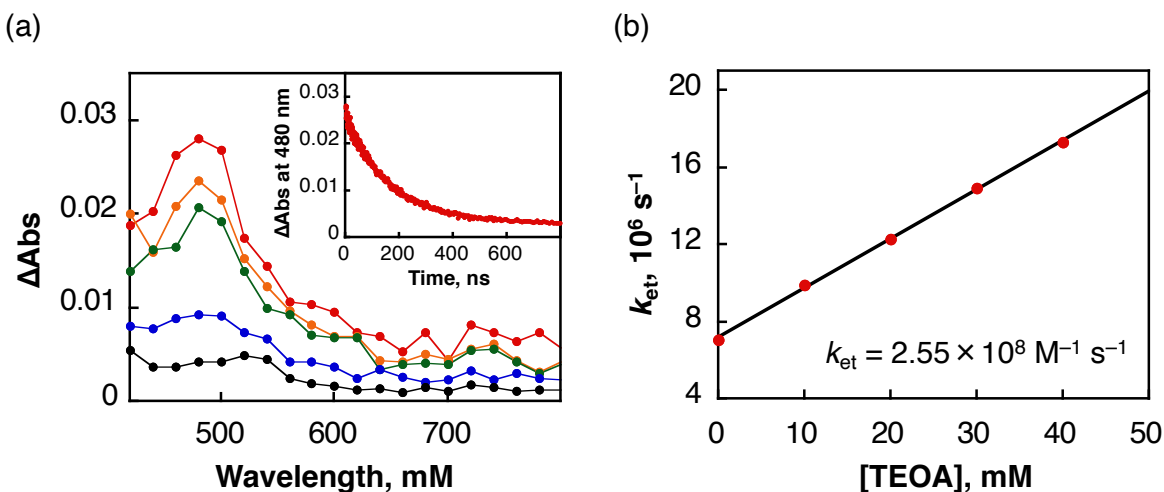


Fig. S14 (a) Transient absorption spectral changes [red (2 ns); orange (20 ns); green (50 ns); blue (200 ns); black (500 ns)] after sub-nanosecond laser excitation at 355 nm in a deaerated DMA solution containing **2** (2.0 mM) at 298 K. Inset shows the decay time profile of the absorbance at 480 nm due to the decay of the excited state of **2**. (b) Plot of k_{obs} vs concentration of TEOA in a DMA solution at 298 K.

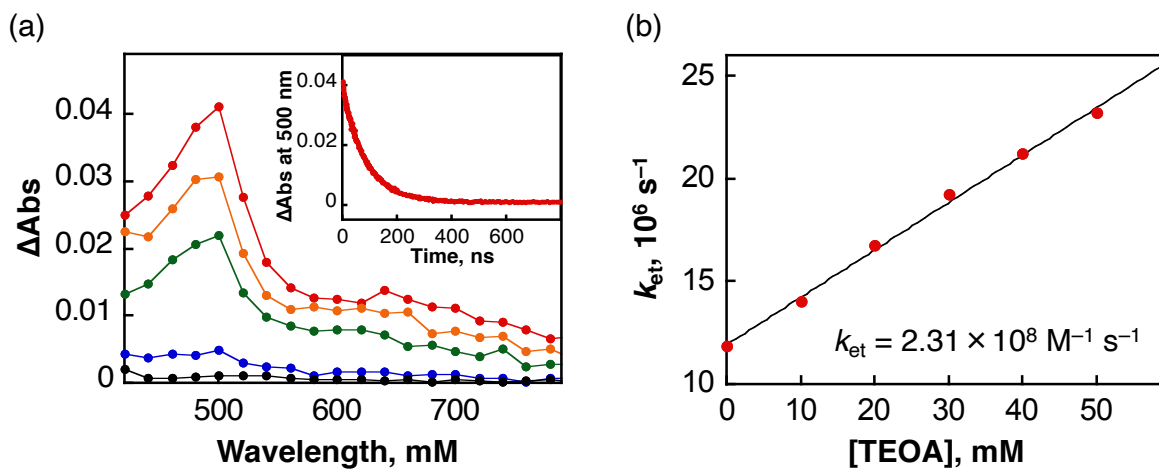


Fig. S15 (a) Transient absorption spectral changes [red (2 ns); orange (20 ns); green (50 ns); blue (200 ns); black (500 ns)] after sub-nanosecond laser excitation at 355 nm in a deaerated DMA solution containing **3** (1.5 mM) at 298 K. Inset shows the decay time profile of the absorbance at 500 nm due to the decay of the excited state of **3**. (b) Plot of k_{obs} vs concentration of TEOA in a DMA solution at 298 K.

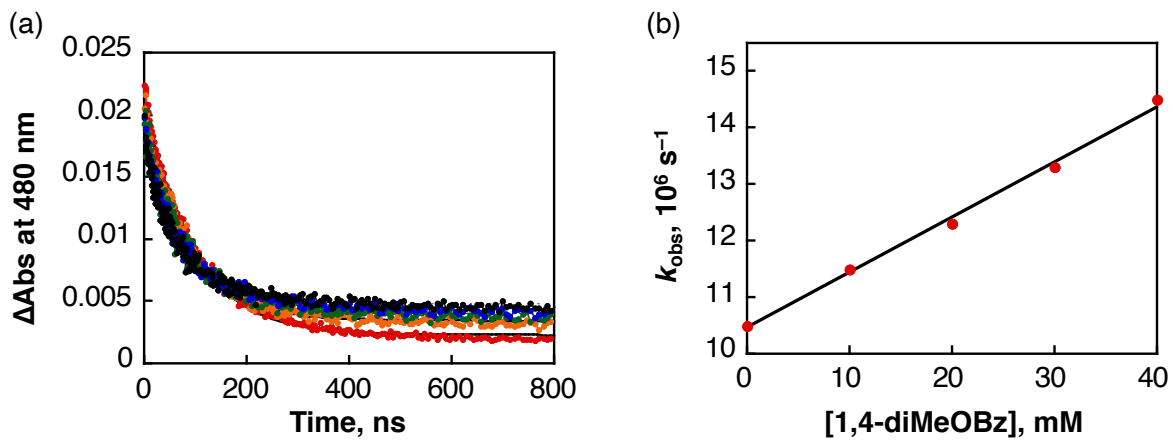


Fig. S16 (a) Decay time profile of the absorbance at 480 nm due to the decay of the excited state of **1** (2.0 mM) in the presence of different concentrations of 1,4-dimethoxybenzene [0 mM (red); 10 mM (orange); 20 mM (green); 30 mM (blue); 40 mM (black)] after sub-nanosecond laser excitation at 355 nm in an Ar-saturated DMA solution containing **1** (2.0 mM) and 1,4-dimethoxybenzene (1,4-diMeOBz, 0–40 mM) at 298 K. (b) Plot of k_{obs} vs concentration of 1,4-dimethoxybenzene in a DMA solution at 298 K.

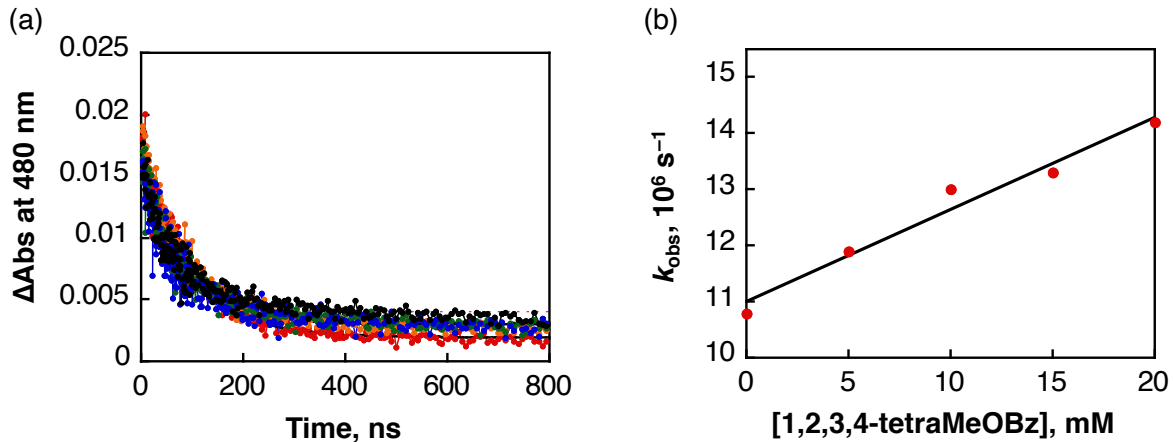


Fig. S17 (a) Decay time profile of the absorbance at 480 nm due to the decay of the excited state of **1** (2.0 mM) in the presence of different concentrations of 1,2,3,4-tetramethoxybenzene [0 mM (red); 5 mM (orange); 10 mM (green); 15 mM (blue); 20 mM (black)] after sub-nanosecond laser excitation at 355 nm in an Ar-saturated DMA solution containing **1** (2.0 mM) and 1,2,3,4-tetramethoxybenzene (1,2,3,4-tetraMeOBz, 0–20 mM) at 298 K. (b) Plot of k_{obs} vs concentration of 1,2,3,4-tetramethoxybenzene in a DMA solution at 298 K.

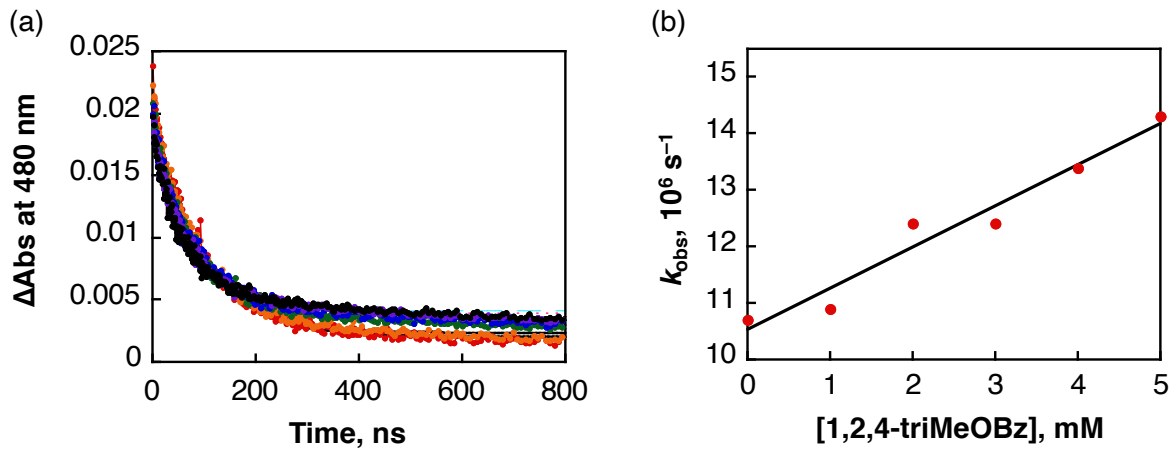


Fig. S18 (a) Decay time profile of the absorbance at 480 nm due to the decay of the excited state of **1** (2.0 mM) in the presence of different concentrations of 1,2,4-trimethoxybenzene [0 mM (red); 1.0 mM (orange); 2.0 mM (green); 3.0 mM (blue); 4.0 mM (purple); 5.0 mM (black)] after sub-nanosecond laser excitation at 355 nm in an Ar-saturated DMA solution containing **1** (2.0 mM) and 1,2,4-trimethoxybenzene (1,2,4-triMeOBz, 0–5.0 mM) at 298 K. (b) Plot of k_{obs} vs concentration of 1,2,4-trimethoxybenzene in a DMA solution at 298 K.

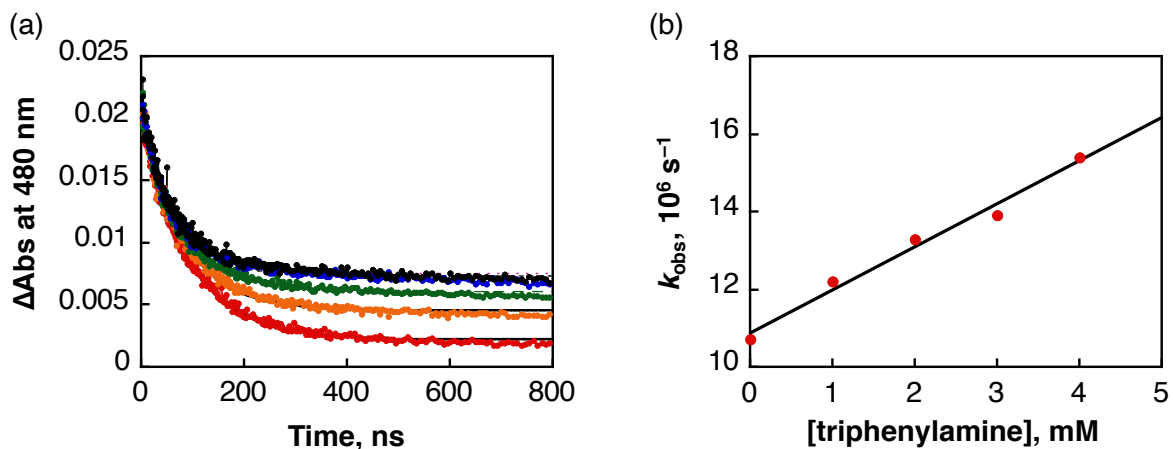


Fig. S19 (a) Decay time profile of the absorbance at 480 nm due to the decay of the excited state of **1** (2.0 mM) in the presence of different concentrations of triphenylamine [0 mM (red); 1.0 mM (orange); 2.0 mM (green); 3.0 mM (blue); 4.0 mM (black)] after sub-nanosecond laser excitation at 355 nm in an Ar-saturated DMA solution containing **1** (2.0 mM) and triphenylamine (0–4.0 mM) at 298 K. (b) Plot of k_{obs} vs concentration of triphenylamine in a DMA solution at 298 K.

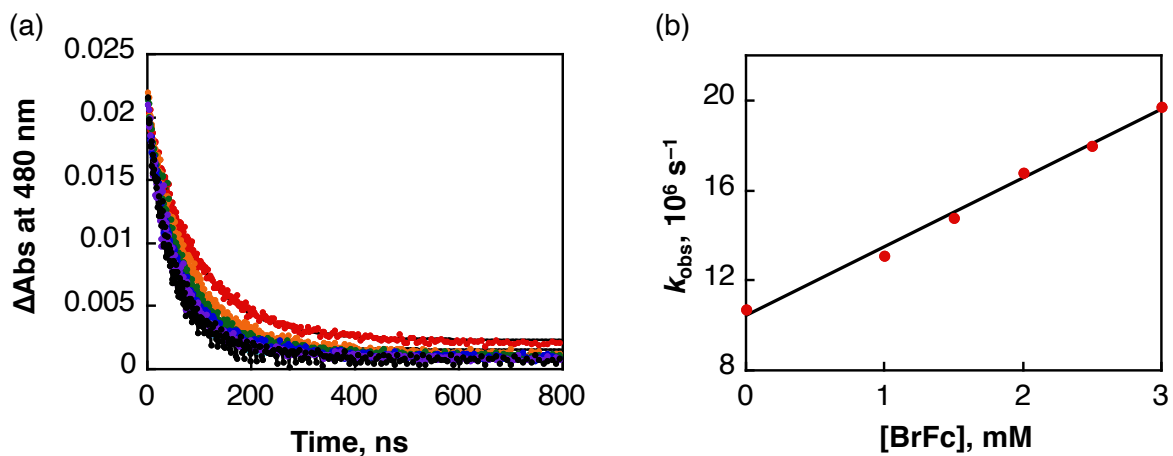


Fig. S20 (a) Decay time profile of the absorbance at 480 nm due to the decay of the excited state of **1** (2.0 mM) in the presence of different concentrations of bromoferrocene [0 mM (red); 1.0 mM (orange); 1.5 mM (green); 2.0 mM (blue); 2.5 mM (purple); 3.0 mM (black)] after sub-nanosecond laser excitation at 355 nm in an Ar-saturated DMA solution containing **1** (2.0 mM) and bromoferrocene (BrFc, 0–3.0 mM) at 298 K. (b) Plot of k_{obs} vs concentration of bromoferrocene in a DMA solution at 298 K.

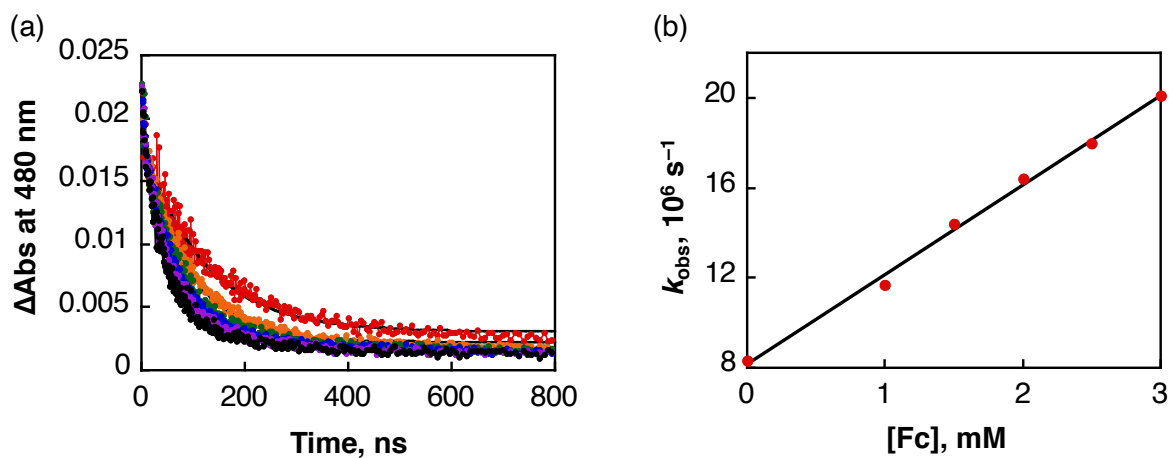


Fig. S21 (a) Decay time profile of the absorbance at 480 nm due to the decay of the excited state of **1** (2.0 mM) in the presence of different concentrations of ferrocene [0 mM (red); 1.0 mM (orange); 1.5 mM (green); 2.0 mM (blue); 2.5 mM (purple); 3.0 mM (black)] after sub-nanosecond laser excitation at 355 nm in an Ar-saturated DMA solution containing **1** (2.0 mM) and ferrocene (0–3.0 mM) at 298 K. (b) Plot of k_{obs} vs concentration of ferrocene in a DMA solution at 298 K.

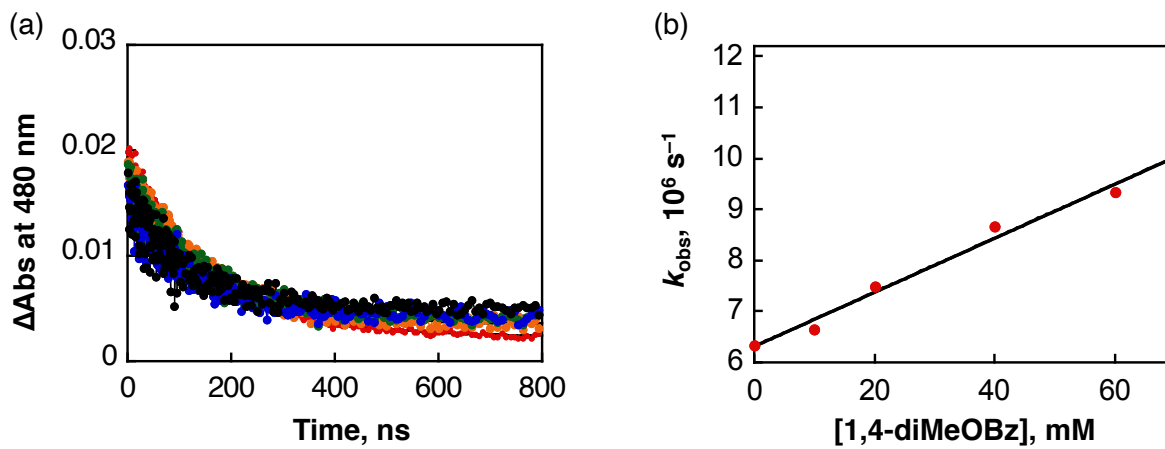


Fig. S22 (a) Decay time profile of the absorbance at 480 nm due to the decay of the excited state of **2** (2.0 mM) in the presence of different concentrations of 1,4-dimethoxybenzene [0 mM (red); 10 mM (orange); 20 mM (green); 40 mM (blue); 60 mM (black)] after sub-nanosecond laser excitation at 355 nm in an Ar-saturated DMA solution containing **2** (2.0 mM) and 1,4-dimethoxybenzene (1,4-diMeOBz, 0–60 mM) at 298 K. (b) Plot of k_{obs} vs concentration of 1,4-dimethoxybenzene in a DMA solution at 298 K.

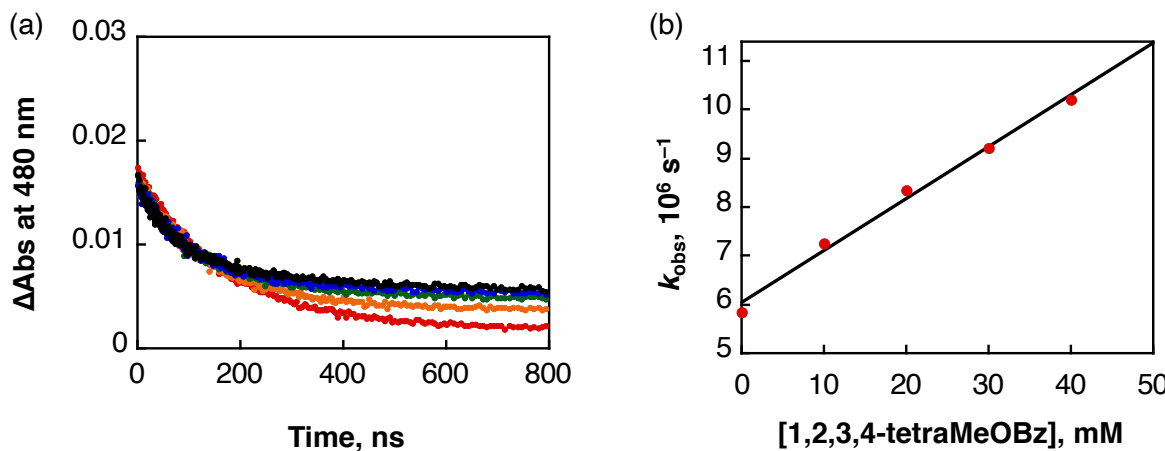


Fig. S23 (a) Decay time profile of the absorbance at 480 nm due to the decay of the excited state of **2** (2.0 mM) in the presence of different concentrations of 1,2,3,4-tetramethoxybenzene [0 mM (red); 10 mM (orange); 20 mM (green); 30 mM (blue); 40 mM (black)] after sub-nanosecond laser excitation at 355 nm in an Ar-saturated DMA solution containing **2** (2.0 mM) and 1,2,3,4-tetramethoxybenzene (1,2,3,4-tetraMeOBz, 0–40 mM) at 298 K. (b) Plot of k_{obs} vs concentration of 1,2,3,4-tetramethoxybenzene in a DMA solution at 298 K.

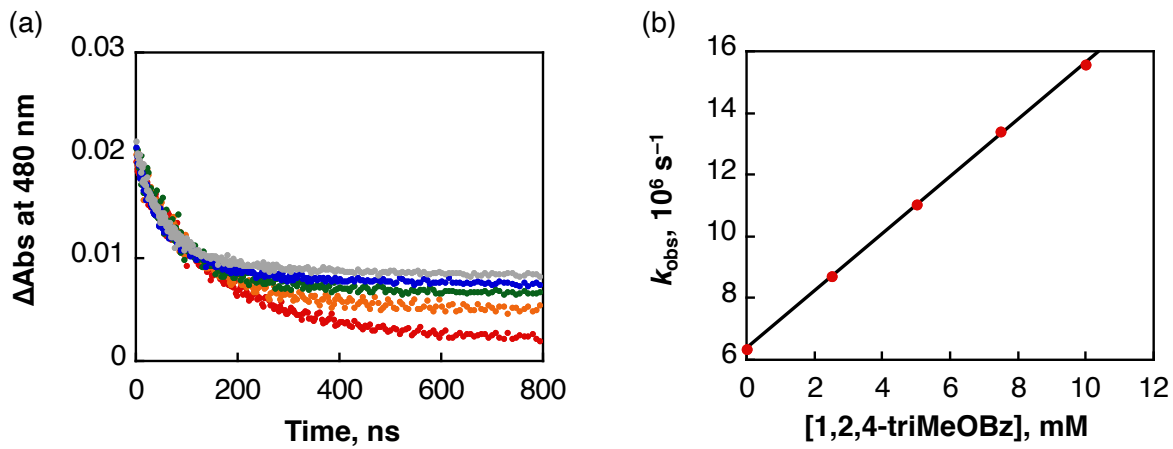


Fig. S24 (a) Decay time profile of the absorbance at 480 nm due to the decay of the excited state of **2** (2.0 mM) in the presence of different concentrations of 1,2,4-trimethoxybenzene [0 mM (red); 2.5 mM (orange); 5.0 mM (green); 7.5 mM (blue); 10 mM (gray)] after sub-nanosecond laser excitation at 355 nm in an Ar-saturated DMA solution containing **2** (2.0 mM) and 1,2,4-trimethoxybenzene (1,2,4-triMeOBz, 0–10 mM) at 298 K. (b) Plot of k_{obs} vs concentration of 1,2,4-trimethoxybenzene in a DMA solution at 298 K.

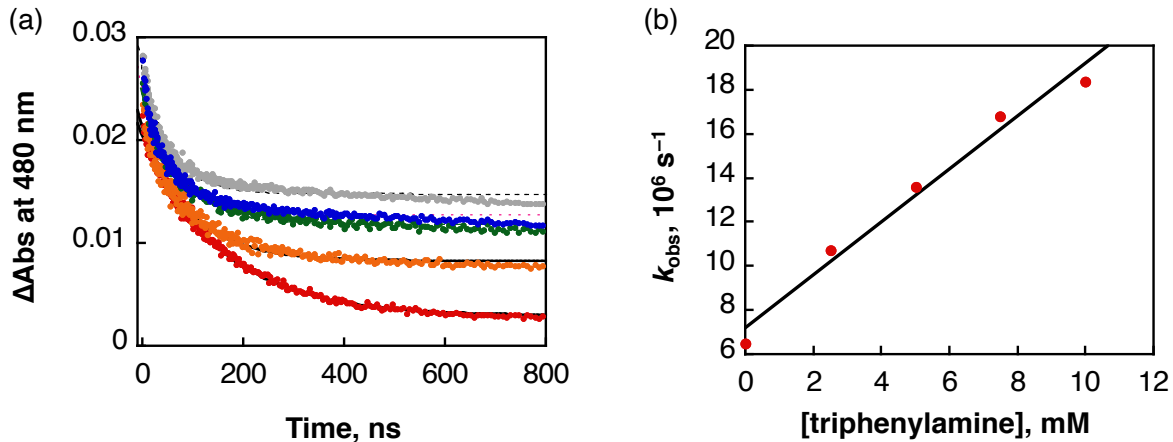


Fig. S25 (a) Decay time profile of the absorbance at 480 nm due to the decay of the excited state of **2** (2.0 mM) in the presence of different concentrations of triphenylamine [0 mM (red); 2.5 mM (orange); 5.0 mM (green); 7.5 mM (blue); 10 mM (gray)] after sub-nanosecond laser excitation at 355 nm in an Ar-saturated DMA solution containing **2** (2.0 mM) and triphenylamine (0–10 mM) at 298 K. (b) Plot of k_{obs} vs concentration of triphenylamine in a DMA solution at 298 K.

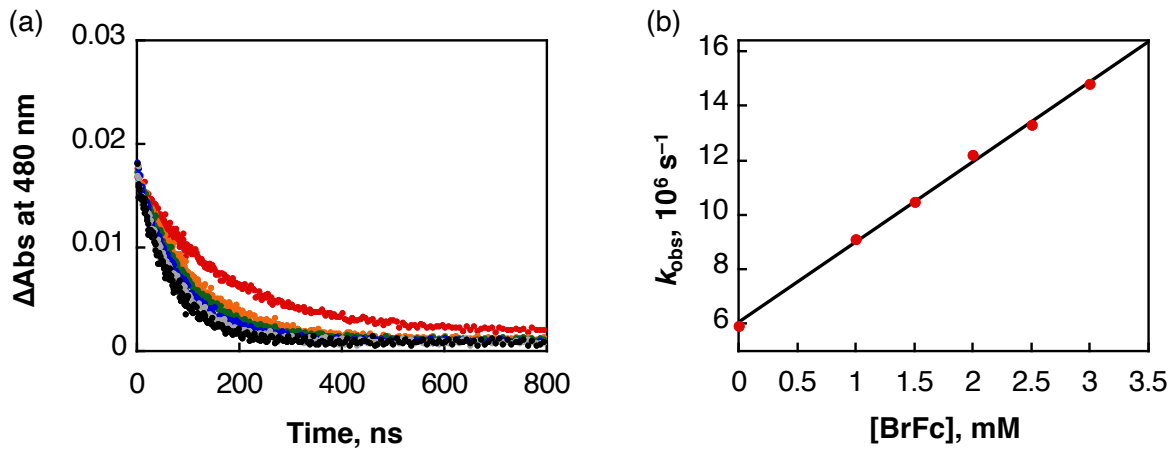


Fig. S26 (a) Decay time profile of the absorbance at 480 nm due to the decay of the excited state of **2** (2.0 mM) in the presence of different concentrations of bromoferrocene [0 mM (red); 1.0 mM (orange); 1.5 mM (green); 2.0 mM (blue); 2.5 mM (gray); 3.0 mM (black)] after sub-nanosecond laser excitation at 355 nm in an Ar-saturated DMA solution containing **2** (2.0 mM) and bromoferrocene (BrFc, 0–3.0 mM) at 298 K. (b) Plot of k_{obs} vs concentration of bromoferrocene in a DMA solution at 298 K.

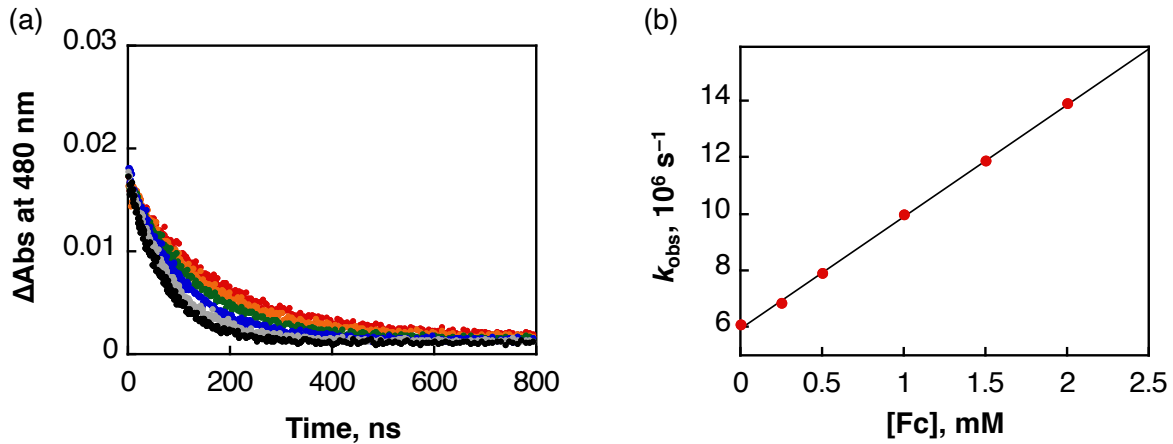


Fig. S27 (a) Decay time profile of the absorbance at 480 nm due to the decay of the excited state of **2** (2.0 mM) in the presence of different concentrations of ferrocene [0 mM (red); 0.25 mM (orange); 0.5 mM (green); 1.0 mM (blue); 1.5 mM (gray); 2.0 mM (black)] after sub-nanosecond laser excitation at 355 nm in an Ar-saturated DMA solution containing **2** (2.0 mM) and ferrocene (0–2.0 mM) at 298 K. (b) Plot of k_{obs} vs concentration of ferrocene in a DMA solution at 298 K.

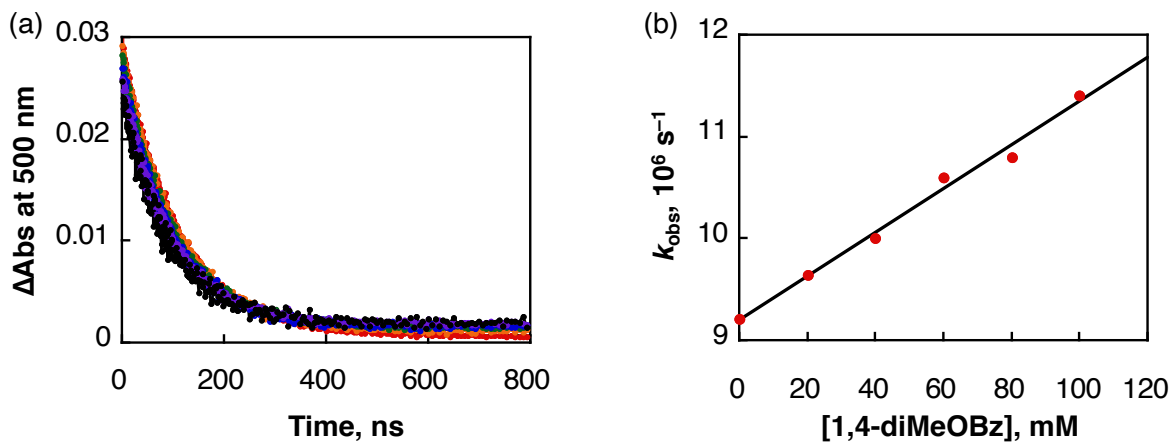


Fig. S28 (a) Decay time profile of the absorbance at 500 nm due to the decay of the excited state of **3** (1.5 mM) in the presence of different concentrations of 1,4-dimethoxybenzene [0 mM (red); 20 mM (orange); 40 mM (green); 60 mM (blue); 80 mM (purple); 100 mM (black)] after sub-nanosecond laser excitation at 355 nm in an Ar-saturated DMA solution containing **3** (1.5 mM) and 1,4-dimethoxybenzene (1,4-diMeOBz, 0–100 mM) at 298 K. (b) Plot of k_{obs} vs concentration of 1,4-dimethoxybenzene in a DMA solution at 298 K.

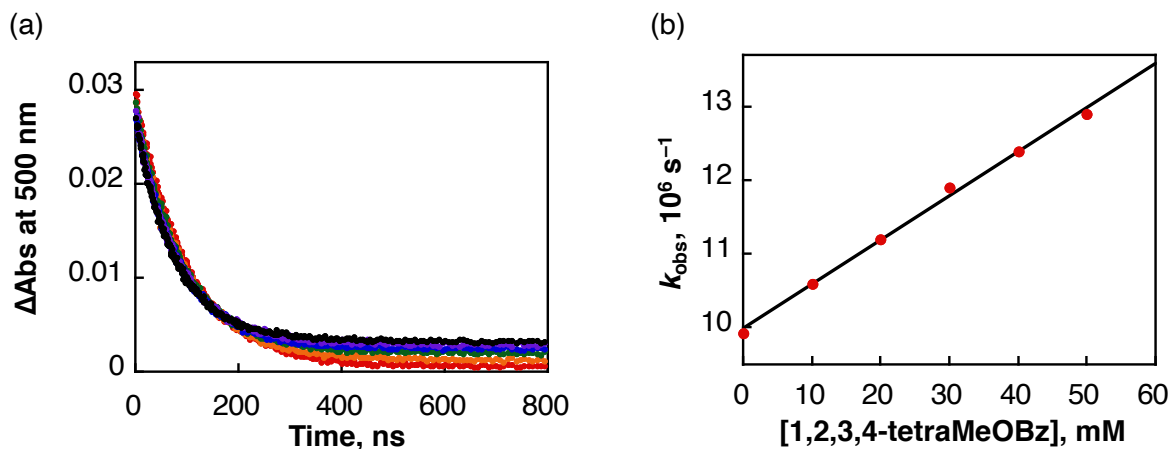


Fig. S29 (a) Decay time profile of the absorbance at 500 nm due to the decay of the excited state of **3** (1.5 mM) in the presence of different concentrations of 1,2,3,4-tetramethoxybenzene [0 mM (red); 10 mM (orange); 20 mM (green); 30 mM (blue); 40 mM (purple); 50 mM (black)] after sub-nanosecond laser excitation at 355 nm in an Ar-saturated DMA solution containing **3** (1.5 mM) and 1,2,3,4-tetramethoxybenzene (1,2,3,4-tetraMeOBz, 0–50 mM) at 298 K. (b) Plot of k_{obs} vs concentration of 1,2,3,4-tetramethoxybenzene in a DMA solution at 298 K.

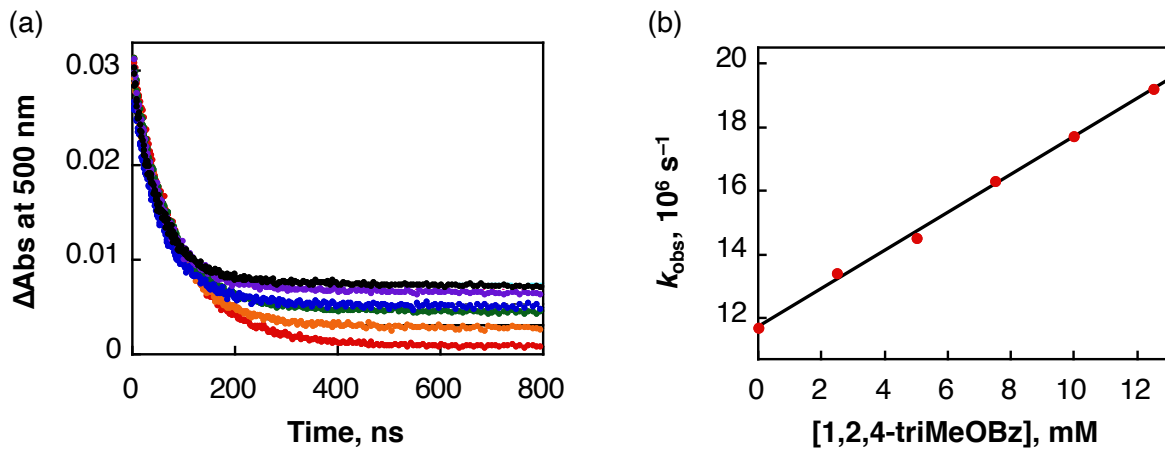


Fig. S30 (a) Decay time profile of the absorbance at 500 nm due to the decay of the excited state of **3** (1.5 mM) in the presence of different concentrations of 1,2,4-trimethoxybenzene [0 mM (red); 2.5 mM (orange); 5.0 mM (green); 7.5 mM (blue); 10.0 mM (purple); 12.5 mM (black)] after sub-nanosecond laser excitation at 355 nm in an Ar-saturated DMA solution containing **3** (1.5 mM) and 1,2,4-trimethoxybenzene (1,2,4-triMeOBz, 0–12.5 mM) at 298 K. (b) Plot of k_{obs} vs concentration of 1,2,4-trimethoxybenzene in a DMA solution at 298 K.

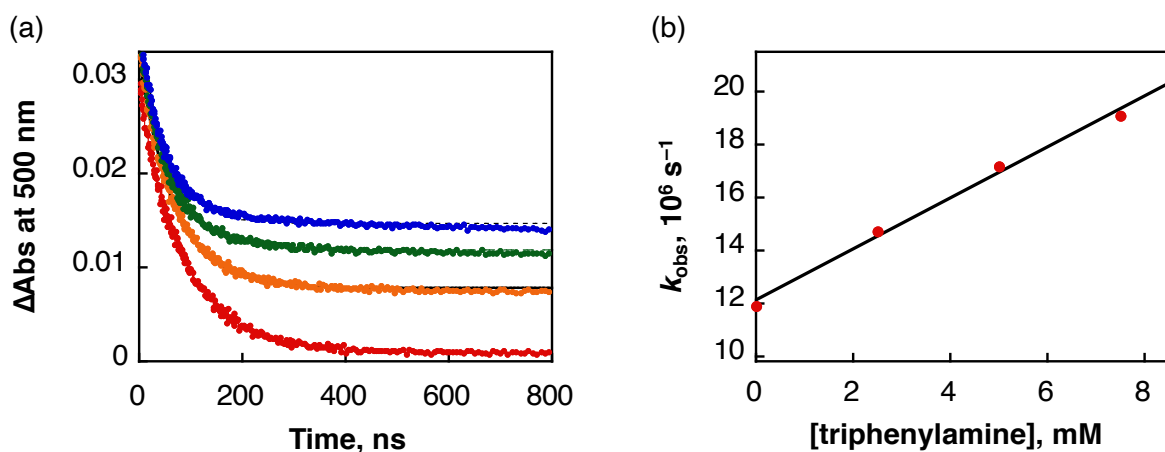


Fig. S31 (a) Decay time profile of the absorbance at 500 nm due to the decay of the excited state of **3** (1.5 mM) in the presence of different concentrations of triphenylamine [0 mM (red); 2.5 mM (orange); 5.0 mM (green); 7.5 mM (blue)] after sub-nanosecond laser excitation at 355 nm in an Ar-saturated DMA solution containing **3** (1.5 mM) and triphenylamine (0–7.5 mM) at 298 K. (b) Plot of k_{obs} vs concentration of triphenylamine in a DMA solution at 298 K.

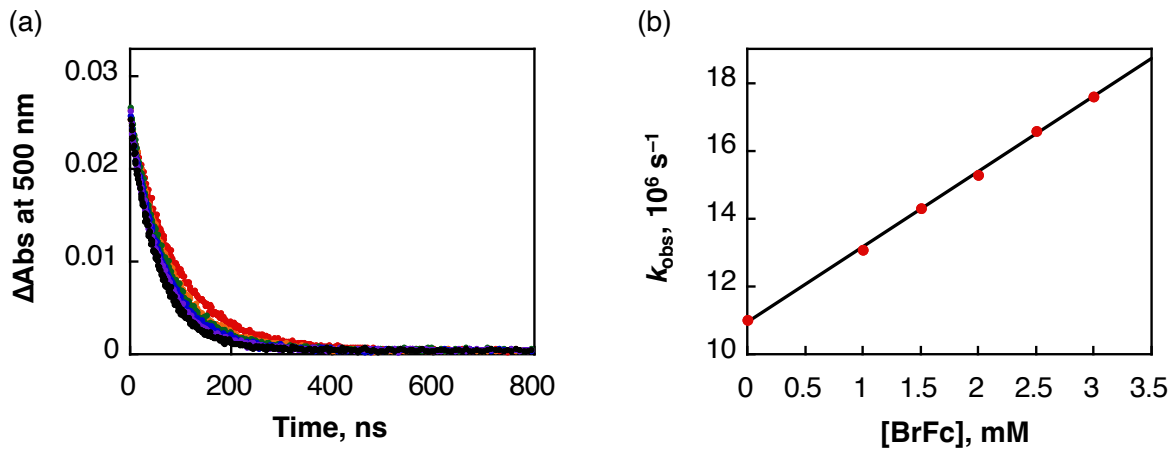


Fig. S32 (a) Decay time profile of the absorbance at 500 nm due to the decay of the excited state of **3** (1.5 mM) in the presence of different concentrations of bromoferrocene [0 mM (red); 1.0 mM (orange); 1.5 mM (green); 2.0 mM (blue); 2.5 mM (purple); 3.0 mM (black)] after sub-nanosecond laser excitation at 355 nm in an Ar-saturated DMA solution containing **3** (1.5 mM) and bromoferrocene (BrFc, 0–3.0 mM) at 298 K. (b) Plot of k_{obs} vs concentration of bromoferrocene in a DMA solution at 298 K.

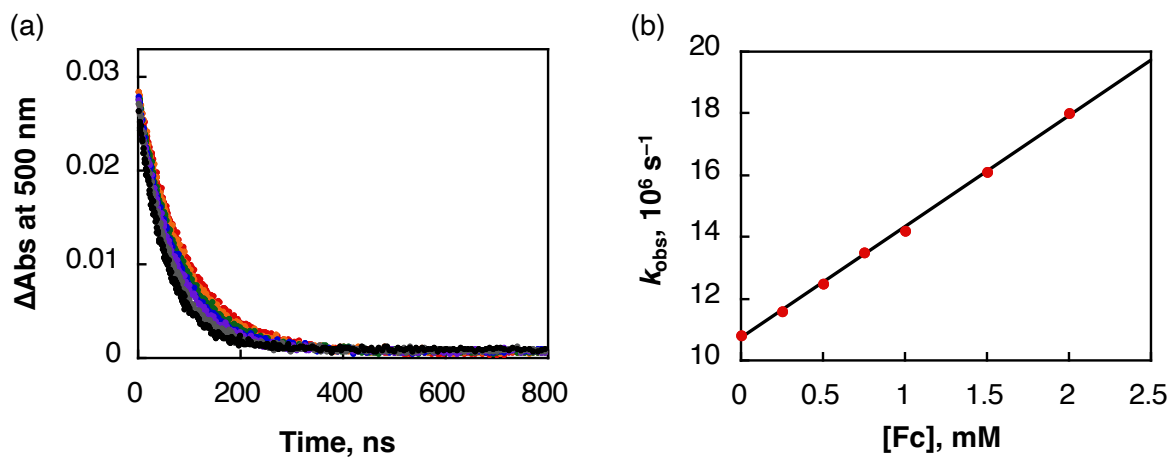


Fig. S33 (a) Decay time profile of the absorbance at 500 nm due to the decay of the excited state of **3** (1.5 mM) in the presence of different concentrations of ferrocene [0 mM (red); 0.25 mM (orange); 0.5 mM (green); 0.75 mM (blue); 1.0 mM (purple); 1.5 mM (gray); 2.0 mM (black)] after sub-nanosecond laser excitation at 355 nm in an Ar-saturated DMA solution containing **3** (1.5 mM) and ferrocene (Fc, 0–3.0 mM) at 298 K. (b) Plot of k_{obs} vs concentration of ferrocene in a DMA solution at 298 K.

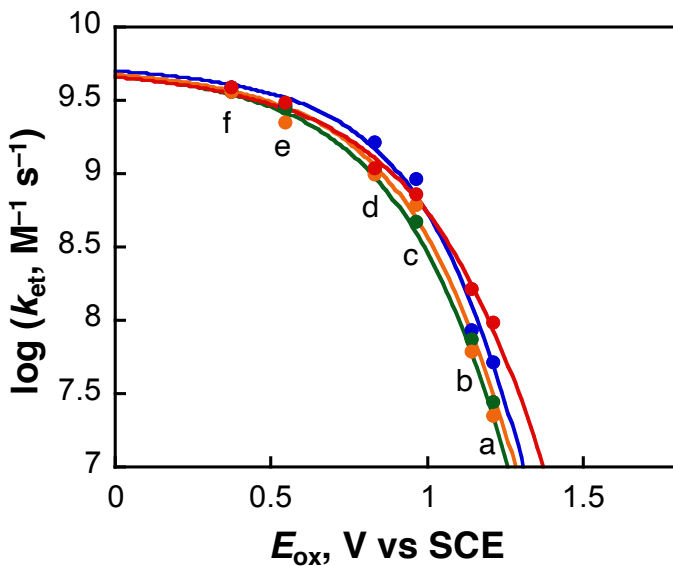


Fig. S34 Plot of $\log k_{\text{et}}$ of photoinduced electron transfer from methoxybenzene derivatives and ferrocene derivatives [a: 1,4-dimethoxybenzene; b: 1,2,3,4-tetramethoxybenzene; c: 1,2,4-trimethoxybenzene; d: triphenylamine; e: bromoferrocene; f: ferrocene] to the excited state of **1** (red), **2** (blue), **3** (orange) and **4** (green)^{S3} in a DMA solution at 298 K. The plot exhibits the expected behavior as expressed by the Marcus equation of intermolecular electron transfer (eq 1):

$$1/k_{\text{et}} = 1/k_{\text{diff}} + 1/(Z \exp[(-\lambda/4)(1 + \Delta G_{\text{et}}/\lambda)^2/(k_B T)]) \quad (1)$$

where λ is the reorganization energy of electron transfer, k_{diff} is the diffusion rate constant, Z is the collision frequency, which is taken as $10^{11} \text{ M}^{-1} \text{ s}^{-1}$, k_B is the Boltzmann constant and T is the absolute temperature.^{S7,S8}

The Gibbs energy change associated with the electron transfer, ΔG_{et} , is given by eq 2:

$$\Delta G_{\text{et}} = e(E_{\text{ox}} - E_{\text{red}}) \quad (2)$$

where e is the elementary charge and E_{red} the one-electron reduction potential of the electron acceptor. The best fit in Fig. S33 gives an E_{red}^* value of 1.47 V, 1.33 V, 1.33 V and 1.32 V as well as a λ of 0.96 eV, 0.85 eV, 0.89 eV, and 0.90 eV for **[1]***, **[2]***, **[3]*** and **[4]***, respectively, along with a k_{diff} of $7.0 \times 10^9 \text{ M}^{-1} \text{ s}^{-1}$. Since the relationship between G_{et} and k_{et} could be explained by nonadiabatic Marcus theory, there are no strong interaction between the excited state of Ir complexes and reductants.

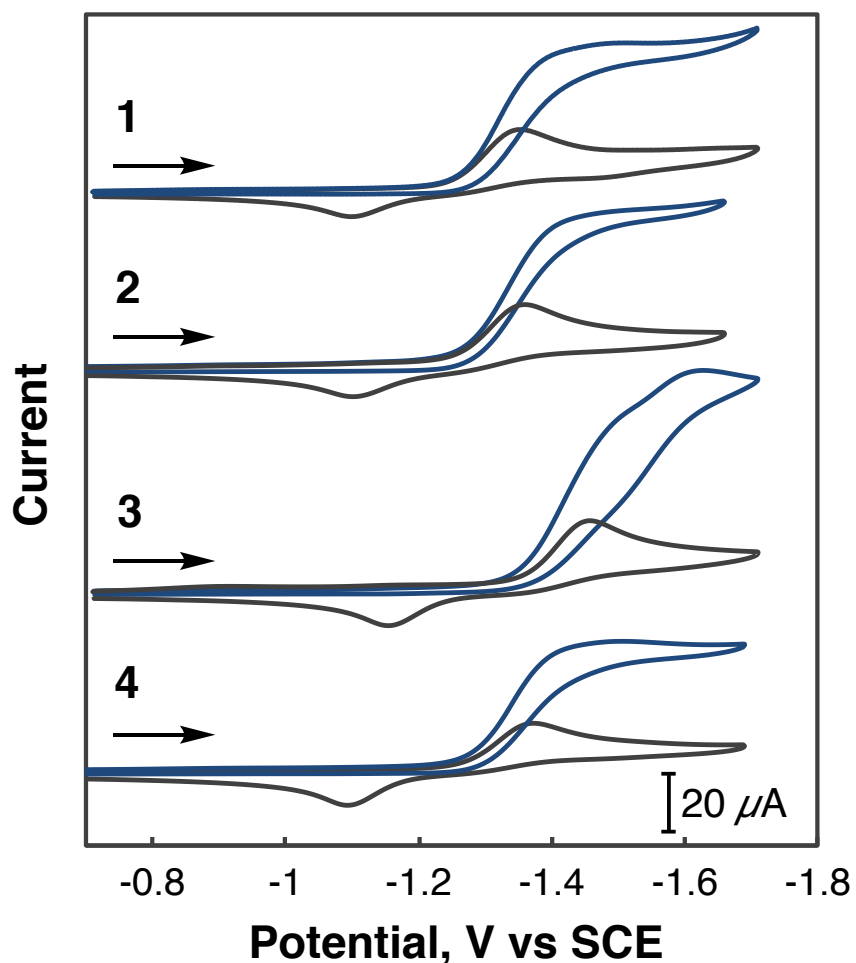


Fig. S35 Cyclic voltammetry of the Ir complexes [1, 2, 3, and 4^{S3}; 1.0 mM] in a DMA solution containing 0.1 M Et₄NBF₄ as a supporting electrolyte and Ag/AgNO₃ (10 mM) as a reference electrode under an Ar atmosphere (black) and a CO₂ atmosphere (blue). Scan rate: 0.1 V s⁻¹.

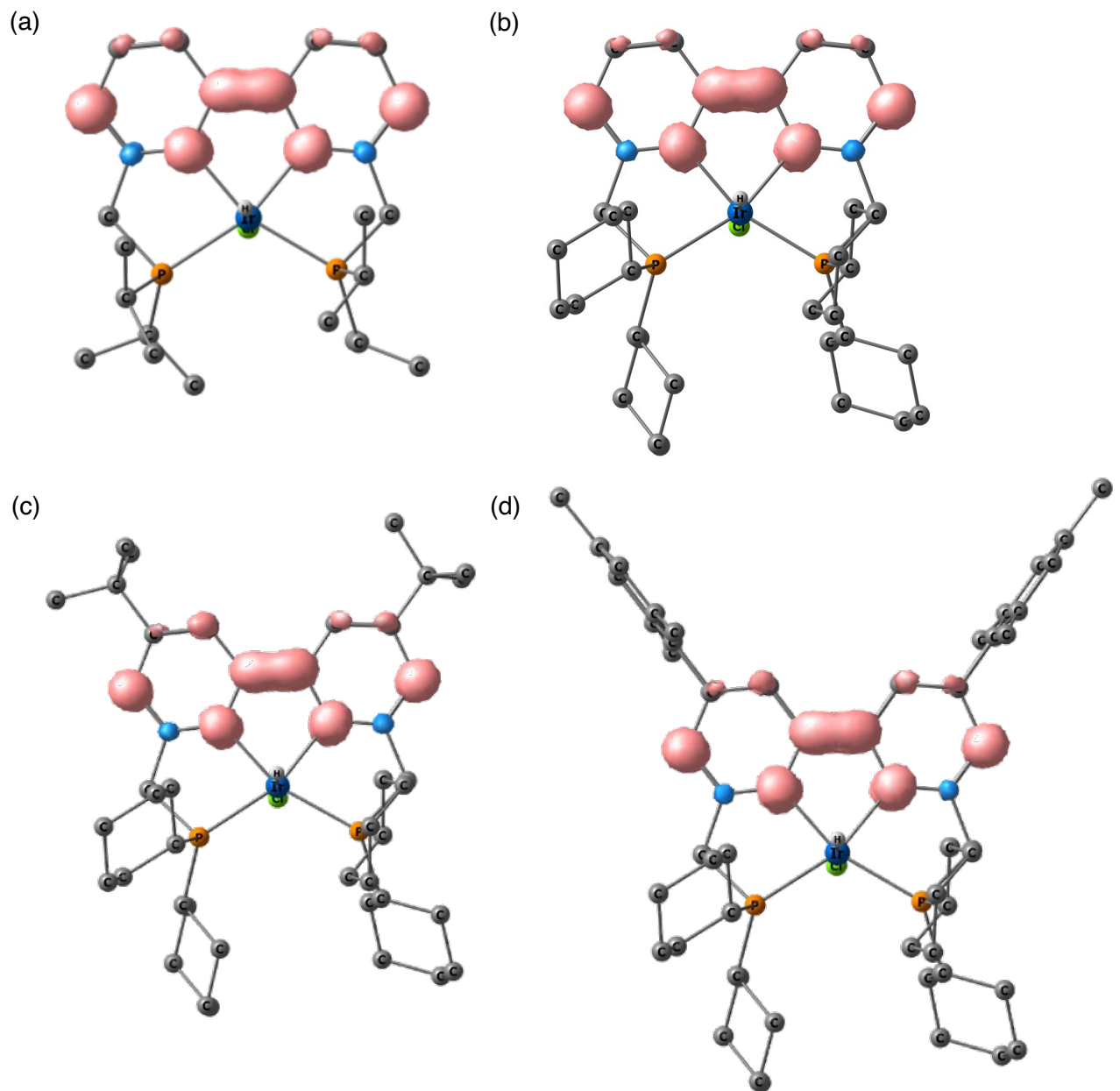


Fig. S36 Spin density distribution in one-electron reduced Ir complexes [(a) 1, (b) 2, (c) 3 and (d) 4].

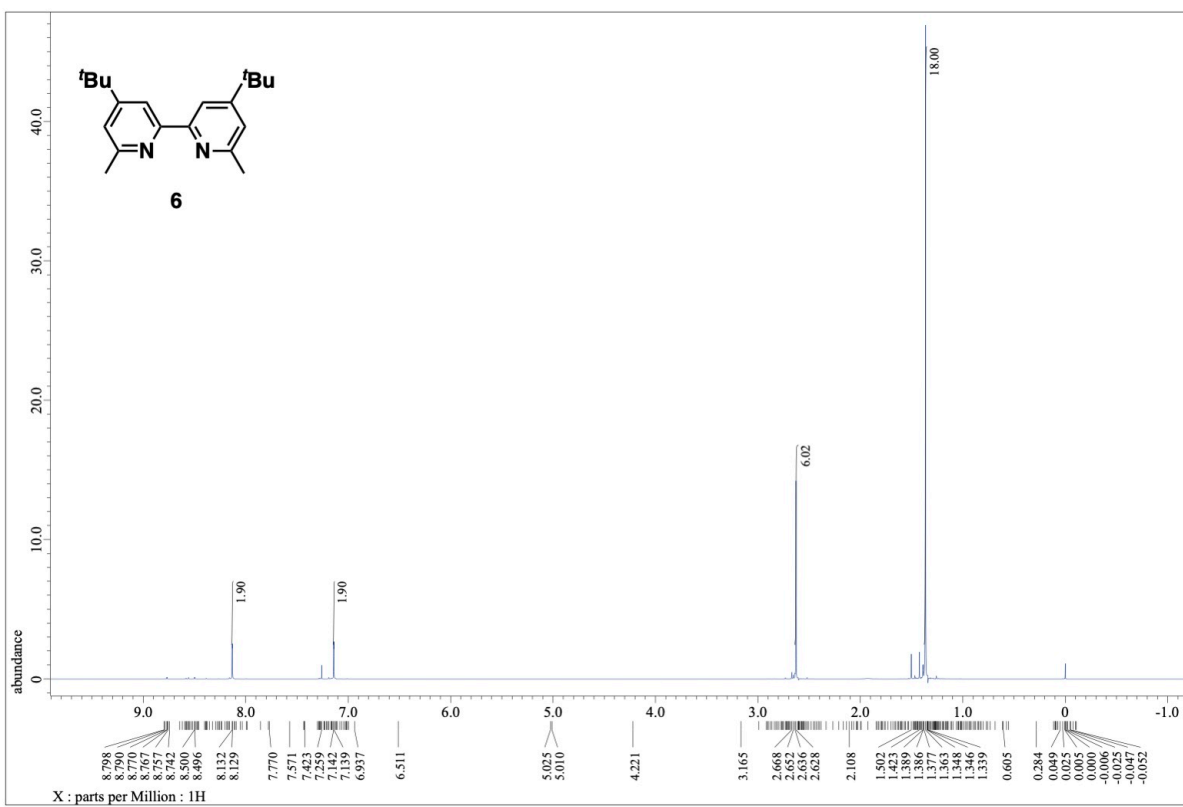


Fig. S37. ¹H NMR spectrum (solvent: CDCl₃) of **6**.

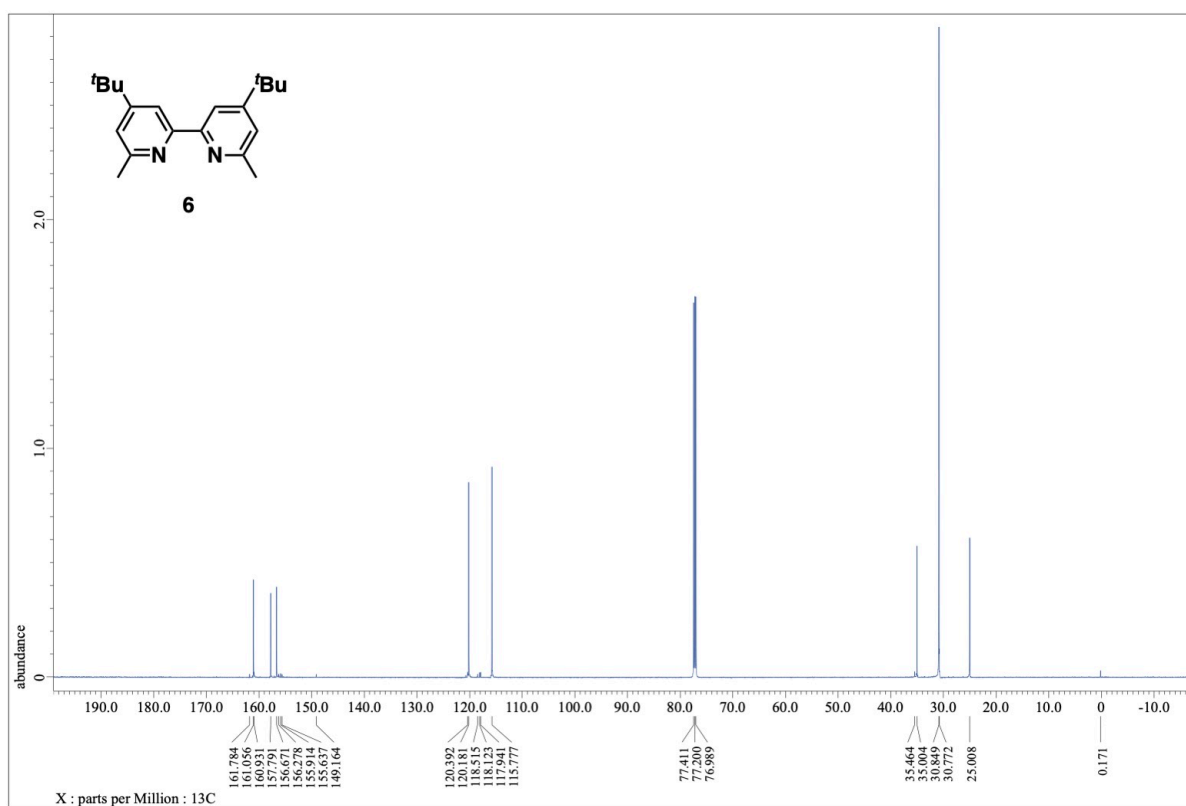


Fig. S38. $^{13}\text{C}\{^1\text{H}\}$ NMR spectrum (solvent: CDCl_3) of **6**.

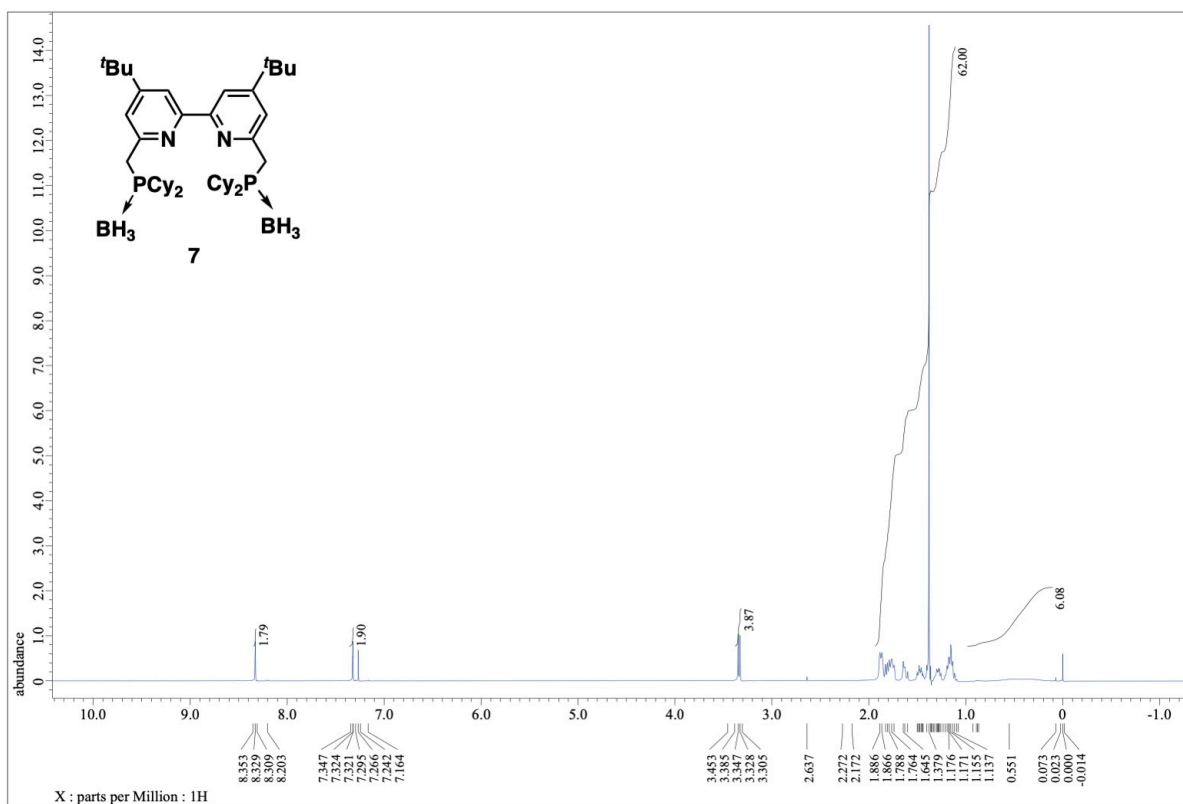


Fig. S39. ^1H NMR spectrum (solvent: CDCl_3) of 7.

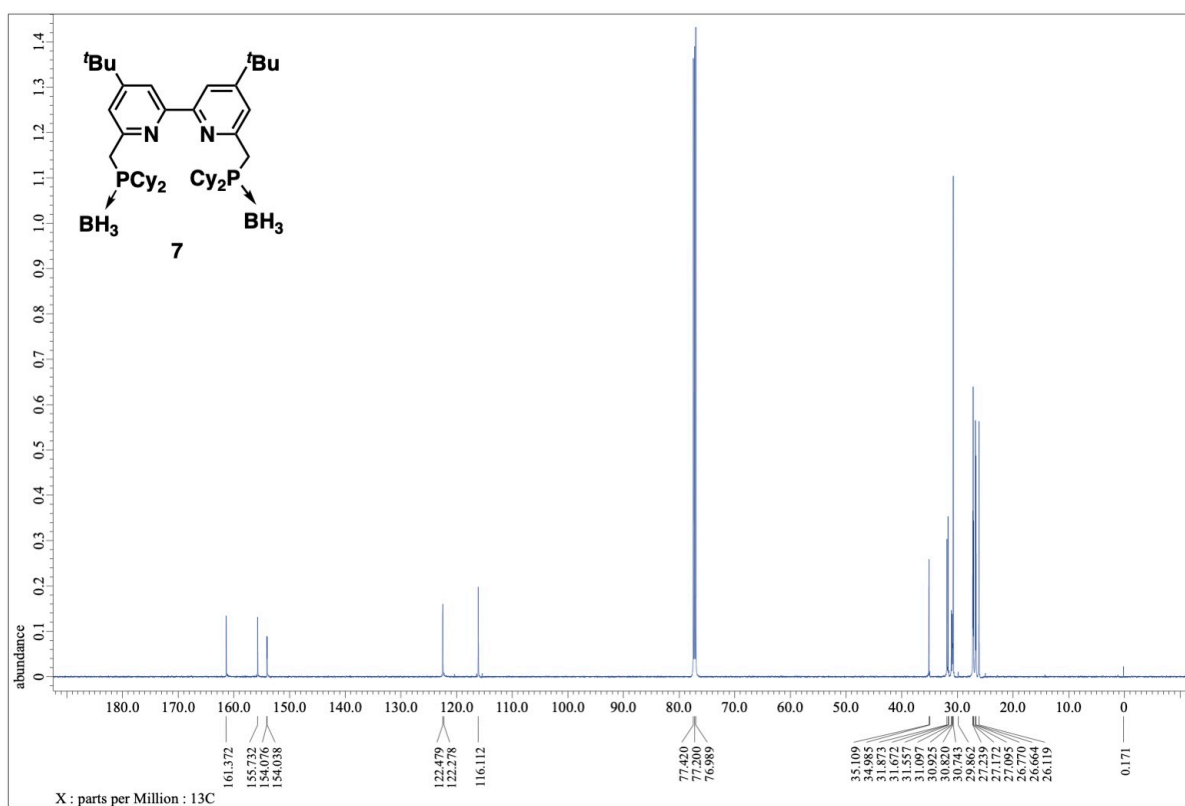


Fig. S40. ¹³C{¹H} NMR spectrum (solvent: CDCl₃) of **7**.

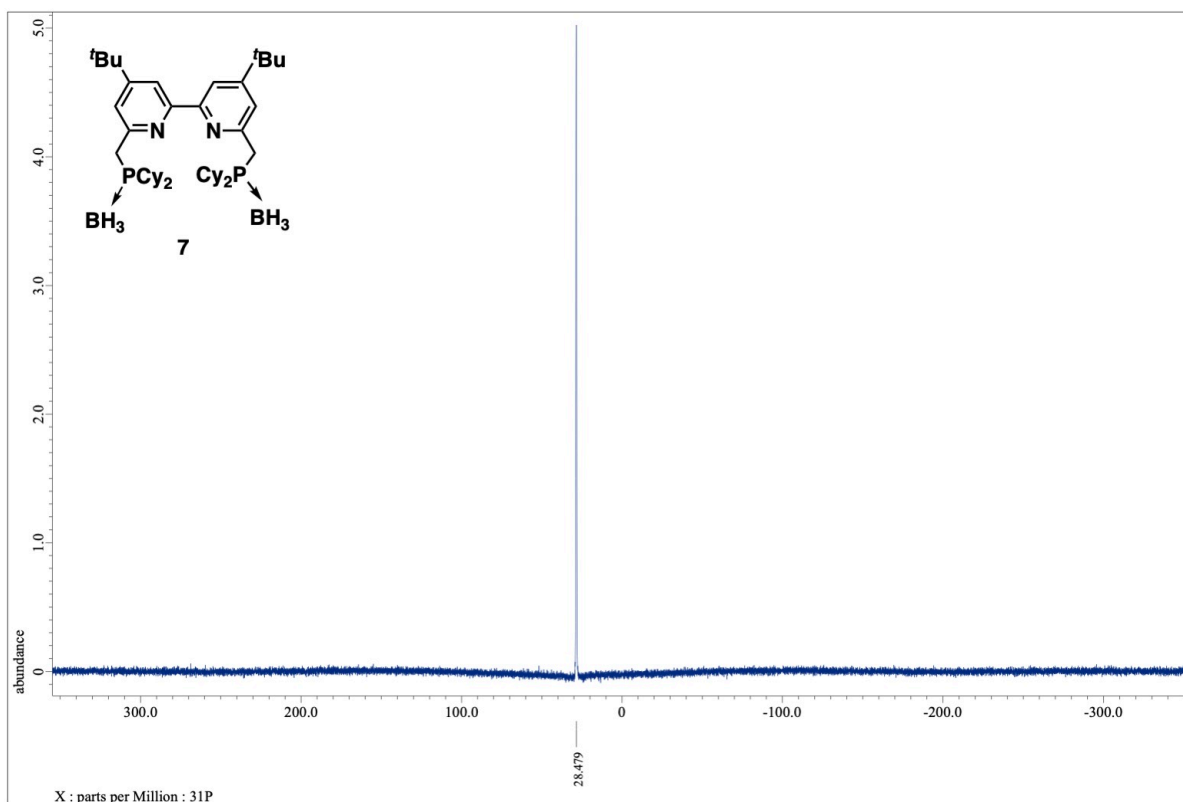


Fig. S41. $^{31}\text{P}\{\text{H}\}$ NMR spectrum (solvent: CDCl_3) of 7.

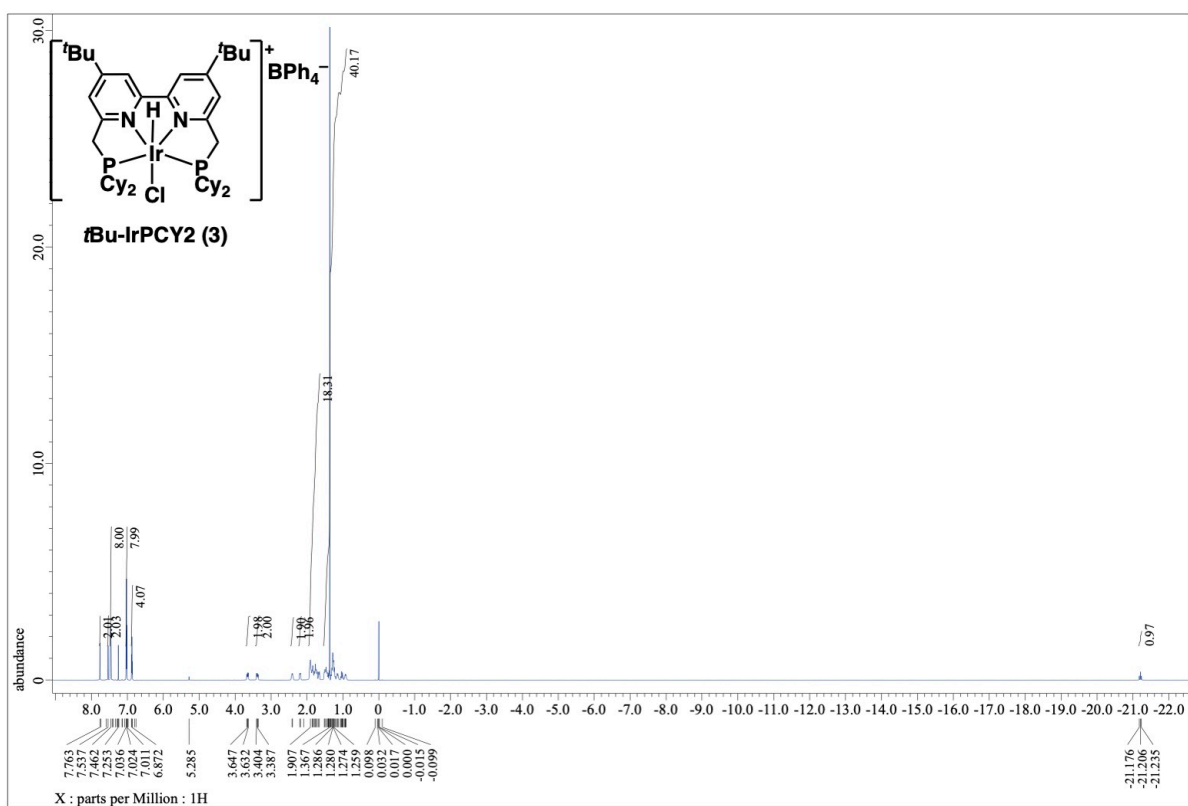


Fig. S42. ^1H NMR spectrum (solvent: CDCl_3) of *t*Bu-IrPCY2.

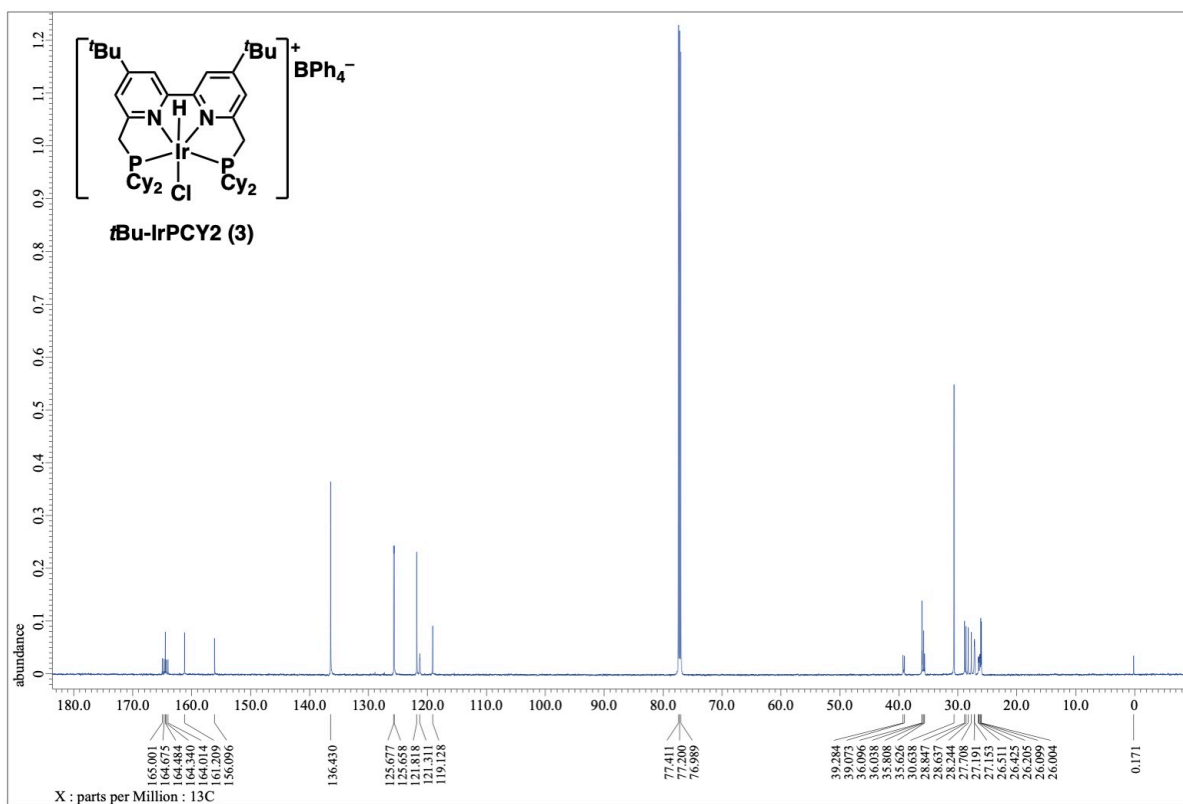


Fig. S43. $^{13}\text{C}\{^1\text{H}\}$ NMR spectrum (solvent: CDCl_3) of *t*Bu-IrPCY2.

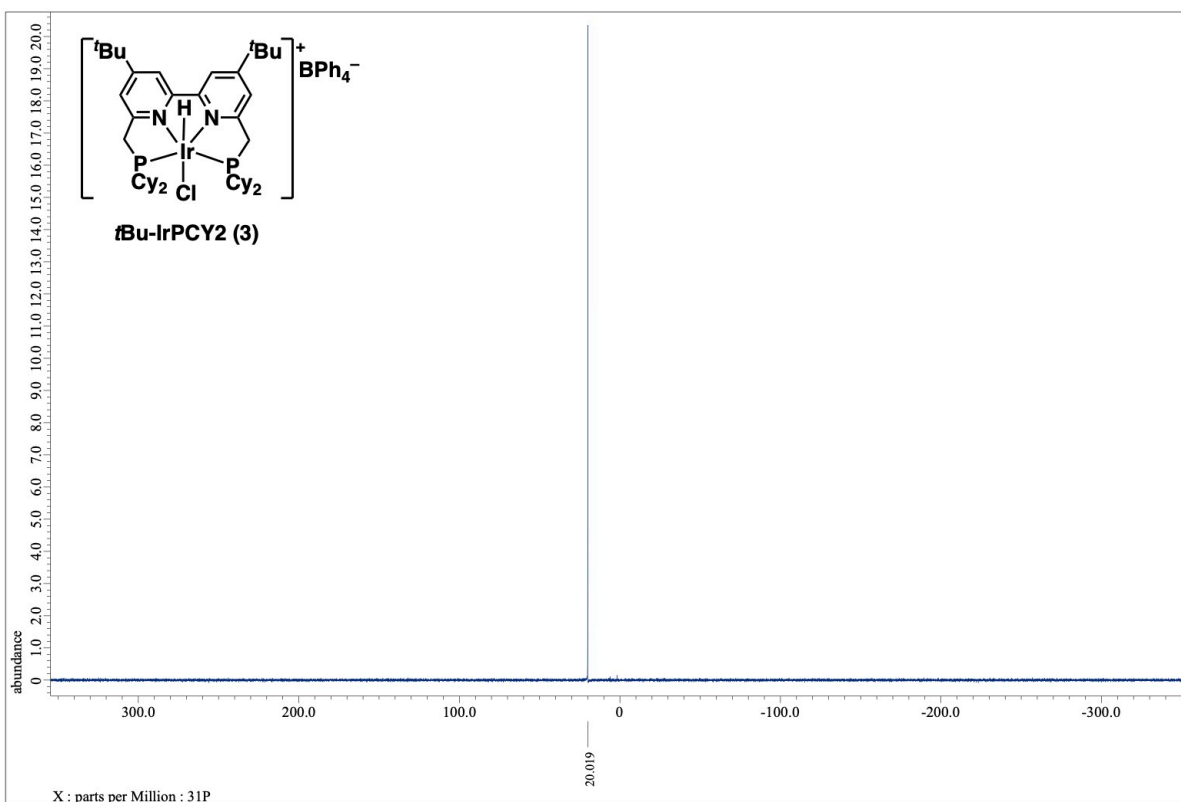


Fig. S44. $^{31}\text{P}\{\text{H}\}$ NMR spectrum (solvent: CDCl_3) of *t*Bu-IrPCY2.

References

- S1 D. Hong, Y. Tsukakoshi, H. Kotani, T. Ishizuka and T. Kojima, *J. Am. Chem. Soc.*, 2017, **139**, 6538–6541.
- S2 S. Yoshioka, S. Nimura, M. Naruto and S. Saito, *Sci. Adv.*, 2020, **6**, eabc0274.
- S3 K. Kamada, J. Jung, T. Wakabayashi, K. Sekizawa, S. Sato, T. Morikawa, S. Fukuzumi and S. Saito, *J. Am. Chem. Soc.*, 2020, **142**, 10261–10266.
- S4 T. Nakagawa, K. Okamoto, H. Hanada and R. Katoh, *Opt. Lett.*, 2016, **41**, 1498–1501.
- S5 C. G. Hatchard and C. A. Parker, *Proc. Roy. Soc. A*, 1956, **235**, 518–536.
- S6 A. D. Becke, *J. Chem. Phys.*, 1993, **98**, 5648-5652.
- S7 C. Lee, W. Yang, R. G. Parr, *Phys. Rev. B*, 1998, 785-789.
- S8 Gaussian 16, Revision C.01, M. J. Frisch, G. W. Trucks, H. B. Schlegel, G. E. Scuseria, M. A. Robb, J. R. Cheeseman, G. Scalmani, V. Barone, G. A. Petersson, H. Nakatsuji, X. Li, M. Cariati, A. V. Marenich, J. Bloino, B. G. Janesko, R. Gomperts, B. Mennucci, H. P. Hratchian, J. V. Ortiz, A. F. Izmaylov, J. L. Sonnenberg, D. Williams-Young, F. Ding, F. Lipparini, F. Egidi, J. Goings, B. Peng, A. Petrone, T. Henderson, D. Ranasinghe, V. G. Zakrzewski, J. Gao, N. Rega, G. Zheng, W. Liang, M. Hada, M. Ehara, K. Toyota, R. Fukuda, J. Hasegawa, M. Ishida, T. Nakajima, Y. Honda, O. Kitao, H. Nakai, T. Vreven, K. Throssell, J. A. Montgomery, Jr., J. E. Peralta, F. Ogliaro, M. J. Bearpark, J. J. Heyd, E. N. Brothers, K. N. Kudin, V. N. Staroverov, T. A. Keith, R. Kobayashi, J. Normand, K. Raghavachari, A. P. Rendell, J. C. Burant, S. S. Iyengar, J. Tomasi, M. Cossi, J. M. Millam, M. Klene, C. Adamo, R. Cammi, J. W. Ochterski, R. L. Martin, K. Morokuma, O. Farkas, J. B. Foresman, and D. J. Fox, Gaussian, Inc., Wallingford CT, 2016.
- S9 D. Andrae, U. Haeussermann, M. Dolg, H. Stoll, H. Preuss, *Theor. Chem. Acc.*, 1990, **77**, 123-141.
- S10 T. H. Dunning Jr. and P. J. Hay, in Modern Theoretical Chemistry, Ed. H. F. Schaefer III, Vol. 3 (Plenum, New York, 1977) 1-28.
- S11 R. Bauernschmitt, R. Ahlrichs, *Chem. Phys. Lett.*, 1996, **256**, 454-464.
- S12 J.-D. Chai, M. Head-Gordon, *Phys. Chem. Chem. Phys.*, 2008, **10**, 6615-6620.
- S13 S. Sato, T. Morikawa, T. Kajino and O. Ishitani, *Angew. Chem., Int. Ed.*, 2013, **52**, 988–992.
- S14 R. O. Reithmeier, S. Meister, B. Riegar, A. Siebel, M. Tschurl, U. Heiz and E. Herdtweck, *Dalton Trans.*, 2014, **43**, 13259–13269.

- S15 A. Genoni, D. N. Chirdon, M. Boniolo, A. Sartorel, S. Bernhard and M. Bonchio, *ACS Catal.*, 2017, **7**, 154–160.
- S16 S. Sato and T. Morikawa, *ChemPhotoChem*, 2018, **2**, 207–212.
- S17 J. Hawecker, J.-M. Lehn and R. Ziessel, *Chem. Commun.*, 1983, **286**, 536–538.
- S18 A. J. Huckaba, E. A. Sharpe and J. H. Delcamp, *Inorg. Chem.*, 2016, **55**, 682–690.
- S19 A. Maurin, C.-O. Ng, L. Chen, T.-C. Lau, M. Robert and C.-C. Ko, *Dalton Trans.*, 2016, **45**, 14524–14529.
- S20 Y. Hameed, P. Berro, B. Gabidullin and D. Richeson, *Chem. Commun.*, 2019, **55**, 11041–11044.
- S21 T. Watanabe, Y. Saga, K. Kosugi, H. Iwami, M. Kondo and S. Masaoka, *Chem. Commun.*, 2022, **58**, 5229–5232.
- S22 S. K. Lee, M. Kondo, M. Okamura, T. Enomoto, G. Nakamura and S. Masaoka, *J. Am. Chem. Soc.*, 2018, **140**, 16899–16903.
- S23 S. Das, R. R. Rodrigues, R. W. Lamb, F. Qu, E. Reinheimer, C. M. Boudreaux, C. E. Webster, J. H. Delcamp and E. T. Papish, *Inorg. Chem.*, 2019, **58**, 8012–8020.
- S24 E. C. Carmen, A. Jennifer, L. Elina, O. Larisa, H. Matti, C. Jérôme, C.-N. Sylvie and D. Alain, *ChemCatChem*, 2016, **8**, 2667–2677.
- S25 J. Bonin, M. Chaussemier, M. Robert and M. Routier, *ChemCatChem*, 2014, **6**, 3200–3207.
- S26 H. Rao, J. Bonin and M. Robert, *Chem. Commun.*, 2017, **53**, 2830–2833.
- S27 D. Behar, T. Dhanasekaran, P. Neta, C. M. Hosten, D. Ejeh, P. Hambright, E. Fujita, *J. Phys. Chem. A* 1998, **102**, 2870–2877.